



OPEN ACCESS

EDITED BY

Noam Greenbaum,
University of Haifa, Israel

REVIEWED BY

Adriana Horbe,
University of Brasilia, Brazil
Bo-Shian Wang,
National Academy of Marine Research
(NAMR), Taiwan

*CORRESPONDENCE

Chongyi E.,
✉ echongyi@163.com,
✉ echongyi@qhnu.edu.cn

SPECIALTY SECTION

This article was submitted to Drylands,
a section of the journal
Frontiers in Environmental Science

RECEIVED 20 October 2022

ACCEPTED 09 January 2023

PUBLISHED 19 January 2023

CITATION

Shi Y, E C, Peng Q, Zhang Z, Zhang J, Yan W
and Xu C (2023), Rare earth elements in
aeolian loess sediments from Menyuan
Basin, northeastern Tibetan plateau:
Implications for provenance.
Front. Environ. Sci. 11:1074909.
doi: 10.3389/fenvs.2023.1074909

COPYRIGHT

© 2023 Shi, E, Peng, Zhang, Zhang, Yan
and Xu. This is an open-access article
distributed under the terms of the [Creative
Commons Attribution License \(CC BY\)](#).
The use, distribution or reproduction in
other forums is permitted, provided the
original author(s) and the copyright
owner(s) are credited and that the original
publication in this journal is cited, in
accordance with accepted academic
practice. No use, distribution or
reproduction is permitted which does not
comply with these terms.

Rare earth elements in aeolian loess sediments from Menyuan Basin, northeastern Tibetan plateau: Implications for provenance

Yunkun Shi^{1,2}, Chongyi E^{1,2,3*}, Qiang Peng^{1,2}, Zhaokang Zhang^{1,2},
Jing Zhang^{1,2}, Wenting Yan⁴ and Chunxia Xu^{1,2}

¹Key Laboratory of Tibetan Plateau Land Surface Processes and Ecological Conservation (Ministry of Education), Qinghai Normal University, Xining, China, ²Qinghai Province Key Laboratory of Physical Geography and Environmental Process, College of Geographical Sciences, Qinghai Normal University, Xining, China, ³Academy of Plateau Science and Sustainability, People's Government of Qinghai Province and Beijing Normal University, Xining, China, ⁴Qinghai Institute of Water Conservancy and Hydropower Research Co., Xining, China

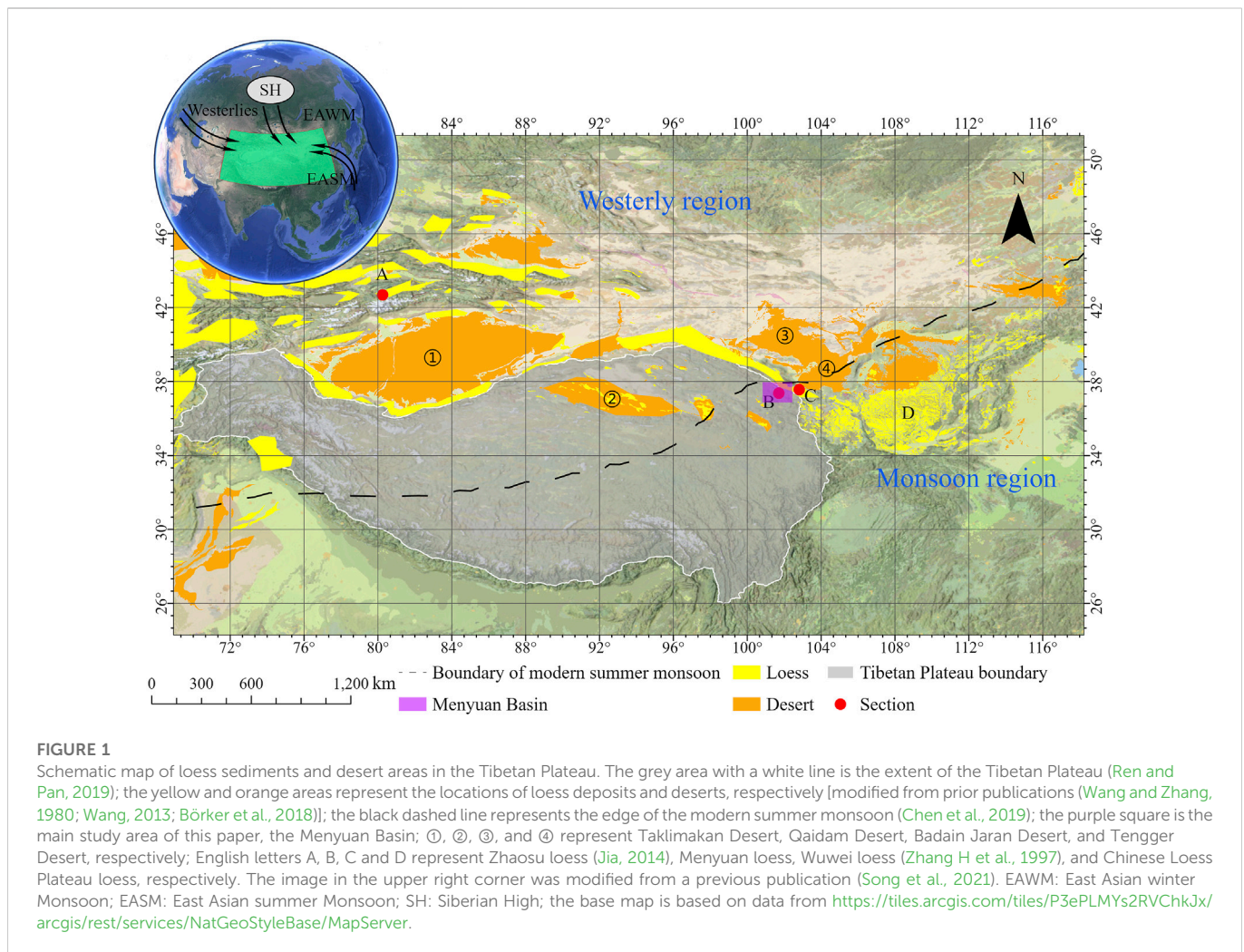
Aeolian loess is a widespread deposit in mid-latitude arid and semiarid regions that has been extensively investigated in arid Central Asia and the Chinese Loess Plateau. The northeastern Tibetan Plateau is crucial to the release, transport, and accumulation of aeolian sediments because of its vast environmental differences, but relatively little research has been conducted on the loess here. To further deepen our understanding of the loess source in this region, we selected the Menyuan Basin as the study area for this loess tracing research. Through our investigation of the indicators and distribution characteristics of rare earth elements in the Yahecun (YHC) loess-paleosol profile of the Menyuan Basin, the following conclusions were drawn: 1) the indices and distribution curves of rare earth elements in the diverse strata of the YHC profile were not significantly distinct and were comparable to those of loess from other locations in northwestern China, revealing a general association with loess in arid northwestern China; 2) the influence of chemical weathering and particle diameter on rare earth elements in the loess of the study area was minimal, and Menyuan loess rare earth elements contained considerable information regarding their source; and 3) a comparison of the $(La/Yb)_N$, δEu , $(La/Sm)_N$, and $(Gd/Yb)_N$ parameters of potential source areas indicates that arid Central Asia, dominated by the Qaidam Desert, is the primary source area of the Menyuan loess, and dust particles released from these deserts are transported to the Menyuan Basin by the Westerlies and deposited to form loess. Additionally, the Badain Jaran Desert is an essential source of material for the Menyuan loess by winter winds, and some Tengger Desert materials are also transported to the Menyuan Basin by winter winds, but the material transported from the Tengger Desert has a negligible contribution.

KEYWORDS

rare earth elements, loess, provenance, Menyuan Basin, northeastern Tibetan Plateau

Introduction

Aeolian loess, a loosely deposited sediment containing silt-sized dust of aeolian origin, is extensively distributed in arid and semi-arid regions of mid-latitudes of both hemispheres (Pye, 1995; Li et al., 2020b; Lu et al., 2022). This material results from physicochemical and mechanical processes, such as erosion, transport, and deposition, which are driven to the



sedimentary site by external inputs (e.g., wind force) from the provenance area (e.g., gobi and desert) (Muhs, 2013; Obrecht et al., 2015; Li et al., 2020a; Li et al., 2020b). Hence, aeolian loess constitutes a unique terrestrial archive containing extensive environmental information on provenance, deposition, and air transport to reveal atmospheric circulation patterns and reconstruct paleoclimate shifts during the Quaternary (E et al., 2018; Sun et al., 2019; Li G et al., 2020; Li P et al., 2022; Miao et al., 2022).

Arid Central Asia and the Chinese Loess Plateau are dotted with large quantities of loess materials, of which researchers have investigated the provenance, formation, and recording environment (Heller and Liu, 1984; An et al., 1991; Sun et al., 2006; E et al., 2012; Li et al., 2018; Wang Y et al., 2020; Song et al., 2021; Kang et al., 2022; Li P et al., 2022). Geochemical evidence, grain size, and other evidence suggests that the loess from the Chinese Loess Plateau predominantly forms from the surrounding desert sands, the Central Asian Orogenic Belt, and the northern Tibetan Plateau while the loess from arid Central Asia primarily comes from the surrounding mountains and desert sands (Zhang et al., 2018; Li et al., 2020b; Li and Song, 2021; Zhang et al., 2022). The northeastern Tibetan Plateau (NETP) is one of the major loess accumulation regions in China (Figure 1) (Lehmkuhl and Haselein, 2000; Stauch et al., 2012). The aeolian loess spans a broad area over various geomorphic NETP surfaces, such as its faulted basins, piedmonts, river terraces, and alluvial-proluvial fans, and their

thicknesses are horizontally discontinuous and vertically inhomogeneous (Tan et al., 2006; Stauch et al., 2012; Lehmkuhl et al., 2014). The NETP is located at the intersection of the East Asian monsoon and mid-latitude westerly atmospheric systems, and the local climate and environment are sensitive and variable (Chen et al., 2016; 2019). Investigating the NETP aeolian loess can improve the understanding of the regional paleoclimate change and paleodust transport processes (Ferrat et al., 2011). As a result, the NETP aeolian loess has received increasing attention.

Rare earth elements are elements with similar physicochemical properties (Wall, 2014; Ramos et al., 2016) and are ubiquitous and less fractionated in diverse sediments. The rare earth elements found in deposits primarily originate from source rocks and are less related to other driving forces, such as weathering, transport, sedimentation, metamorphism, and diagenesis processes (McLennan, 2018). Due to their chemical inertness, rare earth elements are frequently used as tracers (Li et al., 2021). The decomposition and dissolution of rare Earth minerals during physicochemical weathering affect the fractionation of rare earth elements; therefore, certain rare Earth element indicators can record information regarding environmental evolution (Ding et al., 2001). Consequently, rare Earth element signature indicators, such as content, distribution pattern, and differentiation degree, have been extensively employed to investigate loess, lake deposits, and other sediments as significant

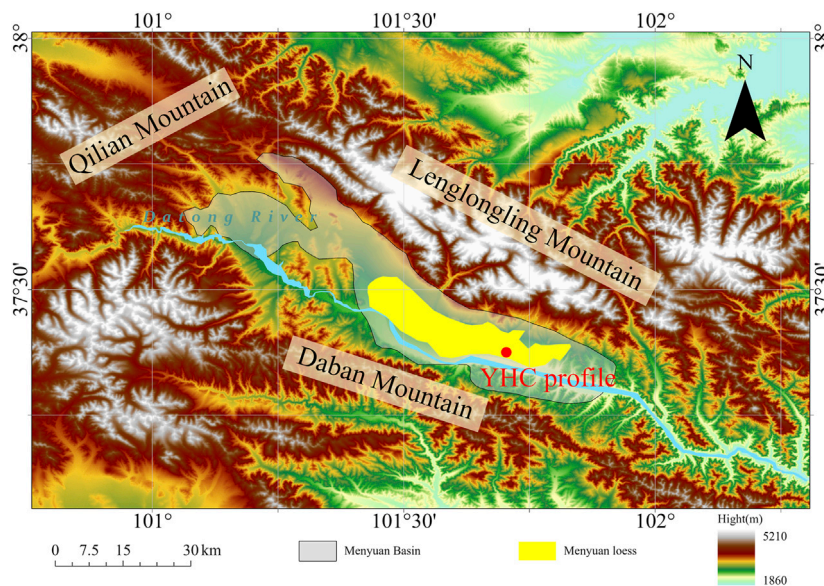


FIGURE 2

Digital elevation model (DEM) of the Menyuan Basin and location of the YHC profile. DEM data from <https://srtm.csi.cgiar.org/>.

proxies to reveal the source, genesis, and sedimentary environment (Jiang et al., 2019; Gallelo et al., 2021; Romero et al., 2021; Zhang X et al., 2021; Deng et al., 2022a).

Previous researchers have conducted work to establish the lithostratigraphy of aeolian loess on the NETP, and most prior research has focused on the chronology, magnetics, and palynology of aeolian loess deposition (Yu and Lai, 2012; Li et al., 2020a; Wei et al., 2020; Shi et al., 2021; Xu et al., 2022); however, minimal research has been conducted on the geochemistry of rare earth elements and their provenance in NETP loess sediments, and only a few studies have indicated that the loess in the NETP may come from within the Tibetan Plateau (Yang et al., 2021). This study, based on the investigation of geochemistry compositions in the loess-paleosol sequence of the Yahecun (YHC) profile in the Menyuan Basin of the NETP, aimed to: 1) characterize rare Earth element features, 2) analyze the controlling rare Earth element factors, and 3) constrain the sediment provenance. This study provides new geochemical results for deciphering paleoenvironmental changes and provenance and deepens our understanding of dust transport and cycle processes to improve the simulation of dust circulation and climate feedback on atmospheric models in high-altitude regions over the long term.

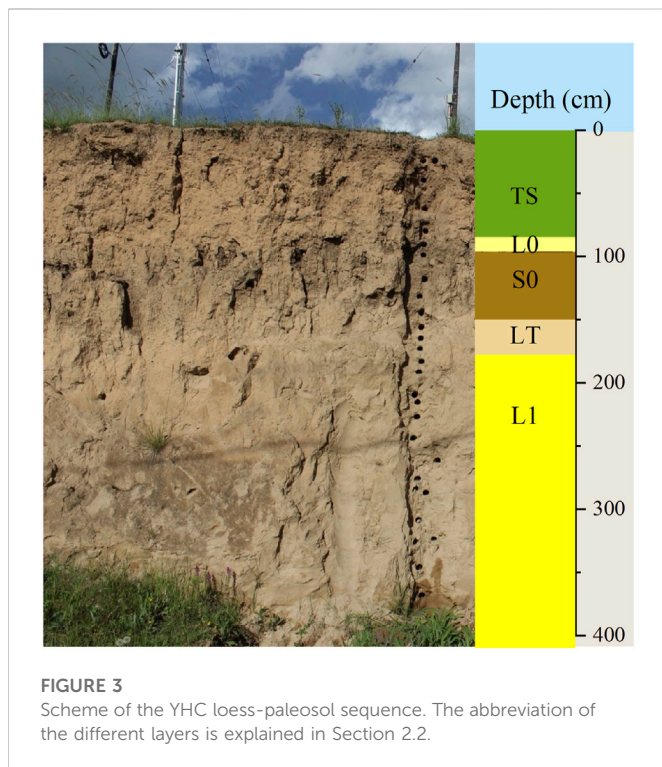
Study area and the profile

Regional setting of Menyuan Basin

The Menyuan Basin (37.16–37.79°N, 101–102°E) is a fault basin located on the NETP in the northwest part of China (Figure 2) that has a breadth of 104 km from north to south, length of approximately 172 km from west to east, and area of approximately 7000 km². The basin slope ranged from northwest to southeast, and its surface elevation ranges from 2900 m in the southeast to 3200 m in the

northwest. Mountains surround the Menyuan Basin in four directions, with the Qilian Mountains in the west, the Lenglongling Mountains in the north and west separating the basin from the Jiuquan–Zhangye Basin and Tengger Desert, and the Konkry Mountains in the south separating it from the Xining Basin. The surrounding mountains are covered with modern glaciers with a 4400 m snowline. Furthermore, several rivers develop from the ambient mountains, including the dominant Datong River, which flows from the Qilian Mountains, through the Menyuan Basin, and to the Huangshui River. The Menyuan Basin, in the marginal zone of the East Asian monsoon and close to the westerly area, is distinguished by a forcefully continental climate. The current annual mean temperature and precipitation in this location are 0.8°C and 526 mm, respectively, with peaks during the summer (Wang et al., 2013).

It is controlled by reverse strike-slip faults in the north and south of the Menyuan Basin, and the altitude difference between the Menyuan Basin and its surrounding mountains is 1100–1500 m because of this faulting. This is evidence that the Menyuan Basin has undergone intense vertical differential movement of marginal faults since the Cenozoic. Near the Menyuan Basin, the outcropping rock strata range from the Ordovician Yingou Formation to the Quaternary system (Ma and Li, 2008). Most of the Menyuan Basin surface layer was covered with thick and various sediments of the Pleistocene, with the thickest being over 400 m, consisting of pluvial-alluvial material, glacial till deposits, and aeolian loess deposits. The aeolian loess is predominantly concentrated on the terrace of the Datong River (Figure 2), dozens of meters thick, dates back to the Middle Pleistocene, and part of it is distributed on the alluvial-proluvial-glacial plain to the east of Haomen Town. The subsurface of the basin comprises reddish Neogene fluviolacustrine mudstone, siltstone, and sandstone overlain by Pleistocene deposits (Wang et al., 2013). Beneath these Pleistocene sediments lies the Miocene fluvial-lacustrine “red layer,” only scantly is exposed near Haomen Town in



the Menyuan Basin, including mudstone, siltstone, and sandstone. Sedimentary facies analyses of the Menyuan Basin show that the sedimentary thickness gradually increases from west to east.

Profile description

Canonically, a type of profile with a stratum of black-brown soil can be observed on Menyuan loess and the YHC profile (101.70 °E, 37.38 °N, [Figure 3](#)) on the second Datong River terrace in the Menyuan Basin was selected as our study area. The YHC profile is located in the northern region of the Yahecun Village and is 2891 m above sea level. The YHC profile, which has an exposed height of 4 m without digging to the bottom of the bedrock, is a fresh longitudinal section resulting from the disinterment of lanes. The stratigraphy of the YHC profile comprises five strata from top to bottom, as follows: 1) topsoil (marked TS), which is a pale brown silty-clay whose formation age is modern and is 82 cm thick with biological channels that comprised some plant roots, such as *Kobresia humilis* and *Potentilla fruticosa*; 2) top loess (marked L0), which is a loose pale-yellow clay layer at approximately 82–96 cm and has a unified texture; 3) paleosol layer (marked S0), which is a brownish-black layer at 96–154 cm and contains abundant finely granular tough and compact structures; 4) transition layer (marked TL), which is 22 cm thick, and is a relatively compact yellowish-brown clay assise with some caliche nodules, that is, a prominent weakly pedogenic layer with a crumbled structure; and 5) lower loess (marked L1), which is a sandy-clay and clay layer which has a similar cooler to L0 and a homogenous structure with loose and obvious vertical joints and is approximately 176–400 cm (the bottom is not exposed) with an existing little caliche nodule at 300–320 cm.

Samples and analytical methods

Sample collection

In the wild, the surface soil of the YHC profile in the vertical direction was cleared by 20 cm to eliminate environmental influence on the protogenous stratum. Professional instruments were used to collect geochemical samples from the top of the YHC profile to the bottom at a 4-cm interval. These scattered samples were then placed in sealed bags marked with information for further laboratory measurements. In total, 100 samples were collected for this study.

Laboratory methods

All fresh material samples underwent natural air drying and were passed through a 20-mesh sieve to remove gravel and biological debris. Then, all samples were ground with a ball mill until they could be passed through a 200-mesh (i.e., approximately 74 μm) sieve.

The rare earth elements were determined using inductively coupled plasma mass spectrometry (iCAP RQ inductively coupled plasma mass spectrometer, Thermo Fisher Scientific, United States) following the standard procedure of GB/T14506.30-2010 at the Xi'an Center of Geological Survey in China Geological Survey, Shanxi, China. In most cases, the relative standard deviation of the measurements was less than 5% for the analyzed elements.

Proxy calculation and data analysis

In nature, elemental abundances exist under odd-even and decreasing rules; therefore, elements in sediments must be normalized. In this study, the chondrite ([Sun and McDonough, 1989](#)) and Upper Continental Crust (UCC) ([Rudnick and Gao, 2003](#)) composition for the normalization of rare earth elements was used to magnify the differentiation degree and reveal the mixed influence of homogenization on the deposition process ([Henderson, 1984](#)).

The following ratios and indices were used in the paper:

$\sum \text{REE}$, LREE, and HREE represent the concentrations of the total rare earth elements, light rare earth elements (from La to Sm), and heavy rare earth elements (from Eu to Lu), respectively. These are the most fundamental properties of rare earth elements in the sediments. LREE/HREE is the ratio of LREE to HREE, indicating the degree of rare earth elements fractionation; the higher the LREE/HREE ratio, the higher the degree of rare earth elements fractionation ([Inguaggiato et al., 2017](#)) $(\text{La}/\text{Yb})_N$ is also a measure of the fractionation degree of rare earth elements, with a high value corresponding to a high rare Earth element fractionation level ([Wei et al., 2018](#)). $(\text{La}/\text{Yb})_N$ is defined by the equation La_N/Yb_N , where “N” is the chondrite-normalized concentration of a particular rare Earth element. $(\text{La}/\text{Sm})_N$ is a measure of the internal fractionation and the overall enrichment in LREE, with the larger the LREEs more obvious the enrichment ([Hao et al., 2010](#)). $(\text{Gd}/\text{Yb})_N$ can reflect HREE depletion and internal fractionation of HREE, with high values indicating a considerable depletion of HREE ([Skurzyński et al., 2020](#)).

δCe , a measurement of Ce anomaly, is the ratio of the observed Ce abundance to its theoretical abundance using the equation $\text{Ce}_N/((\text{La}_N * \text{Pr}_N)^{1/2})$ ([Zhang W et al., 2021](#)). Under oxidation

TABLE 1 The rare earth elements concentrations and parameters in samples from different strata in YHC profile and other areas.

	TS	L0	S0	LT	L1	Menyuan loess	China loess plateau loess	Zhaosu loess	Wuwei loess	Badain jaran desert	Qaidam desert	Taklimakan desert	Tengger desert	UCC	Chondrite
La ($\mu\text{g/g}$)	33.22	33.42	33.58	31.41	32.15	32.57	33.55	37.43	39.59	42.63	38.86	37.31	33.82	31	0.237
Ce ($\mu\text{g/g}$)	67.8	68.83	69.75	64.95	65.04	66.40	64.54	70.07	76.19	92.41	79.82	77.71	72.52	63	0.612
Pr ($\mu\text{g/g}$)	8.04	8.12	8.09	7.53	7.68	7.82	7.82	7.95	8.49	10.11	9.29	8.81	8.08	7.1	0.095
Nd ($\mu\text{g/g}$)	27.75	27.77	28.22	26.39	26.93	27.28	24.83	29.71	32.94	21.61	19.91	22.91	19.33	27	0.467
Sm ($\mu\text{g/g}$)	5.58	5.63	5.67	5.3	5.42	5.49	5.66	5.66	6.44	6.91	6.62	6.3	5.83	4.7	0.153
Eu ($\mu\text{g/g}$)	1.16	1.14	1.14	1.1	1.09	1.11	1.1	1.16	1.3	1.18	1.26	1.19	1.08	1	0.058
Gd ($\mu\text{g/g}$)	5.15	5.16	5.16	4.75	4.9	4.99	5.27	5.11	5.12	5.95	6.03	5.97	5.4	4	0.2055
Tb ($\mu\text{g/g}$)	0.8	0.8	0.79	0.73	0.77	0.78	0.79	0.81	0.89	0.95	0.97	0.89	0.89	0.7	0.0374
Dy ($\mu\text{g/g}$)	4.54	4.59	4.48	4.13	4.36	4.40	4.59	4.65	6.04	5.66	5.75	5.05	5.47	3.9	0.254
Ho ($\mu\text{g/g}$)	0.86	0.85	0.84	0.78	0.83	0.83	0.96	0.92	1.12	1.18	1.19	1.02	1.17	0.83	0.0566
Er ($\mu\text{g/g}$)	2.38	2.34	2.34	2.21	2.27	2.30	2.7	2.77	3.19	3.53	3.42	3.03	3.48	2.3	0.1655
Tm ($\mu\text{g/g}$)	0.36	0.35	0.35	0.33	0.34	0.35	0.43	0.42	0.46	0.55	0.52	0.45	0.55	0.3	0.0255
Yb ($\mu\text{g/g}$)	2.53	2.5	2.47	2.33	2.43	2.45	2.64	2.75	2.84	3.7	3.34	3.02	3.6	2	0.17
Lu ($\mu\text{g/g}$)	0.36	0.35	0.35	0.32	0.34	0.34	0.4	0.41	0.43	0.57	0.5	0.45	0.55	0.31	0.0254
ΣREE ($\mu\text{g/g}$)	160.53	161.86	163.23	152.26	154.54	157.11	155.28	169.81	185.04	196.94	177.5	174.1	161.78	148.14	2.5619
LREE ($\mu\text{g/g}$)	143.55	144.91	146.45	136.68	138.32	140.67	137.49	151.98	164.95	174.84	155.77	154.24	140.66	133.8	1.622
HREE ($\mu\text{g/g}$)	16.98	16.94	16.78	15.58	16.22	16.44	17.78	17.83	20.09	22.09	21.73	19.87	21.11	14.34	0.9399
LREE/HREE	8.46	8.55	8.73	8.77	8.52	8.57	7.79	8.51	8.24	8.16	7.27	7.68	6.81	9.33	1.73
δEu	0.64	0.65	0.65	0.63	0.64	0.64	0.61	0.66	0.69	0.59	0.62	0.63	0.6	0.71	1
δCe	1.02	1.02	1.04	1.04	1.02	1.02	0.98	1	1.02	1.1	1.03	1.05	1.07	1.04	1
$(\text{La/Yb})_N$	9.41	9.58	9.76	9.68	9.52	9.54	9.23	9.76	10.1	8.82	8.46	8.83	7.09	11.12	1
$(\text{La/Sm})_N$	3.82	3.84	3.82	3.83	3.85	3.84	3.82	4.27	3.97	4.01	3.75	3.76	3.74	4.26	1
$(\text{Gd/Yb})_N$	1.68	1.71	1.73	1.69	1.68	1.69	1.67	1.54	1.5	1.41	1.54	1.73	1.32	1.65	1
References	This study	Chen et al. (1996); Ferrat et al. (2011); Zhang et al. (2018)	Jia, (2014)	Zhang H et al. (1997)	Ferrat et al. (2011); Zhang et al. (2018)	Ferrat et al. (2011); Ling et al. (2018); Zhang et al. (2018)	Ferrat et al. (2011); Zhang et al. (2018)	Ferrat et al. (2011); Zhang et al. (2018)	Rudnick and Gao, (2003)	Sun and McDonough, (1989)					

conditions, Ce is oxidized from Ce^{3+} to a stable tetravalent state (Ce^{4+}), which frequently separates from other LREE on the weathered surface, resulting in Ce enrichment and an increase in the δCe value; therefore, δCe can reflect the weathering and pedogenesis in the stratum (Li et al., 2017; Skurzyński et al., 2020). High δCe values indicate considerable weathering and pedogenesis, the δCe anomalies are judged to be bounded by 0.95 and 1.05, with a value greater than 1.05, indicating a positive anomaly, and a value less than 0.95, suggesting a negative anomaly (Chen et al., 2021).

δEu , defined by the equation $\delta Eu = Eu_N / ((Sm_N * Gd_N)^{1/2})$, is a measure of the Eu anomaly (Zhang W et al., 2021). Compared with other rare earth elements, except for the case of strong enrichment of plagioclase, δEu is relatively stable in nature, and the source rock type predominantly determines the value of δEu ; therefore, δEu can be used as an indicator of provenance change (Li et al., 2021). The boundary of the δEu anomaly is consistent with the δCe anomaly, with a δEu greater than 1.05 representing a positive anomaly and a δEu value less than 0.95 being a negative anomaly (Chen et al., 2021).

Results

Various stratigraphic laboratory data of rare earth elements ($\mu g/g$) measured in the YHC sediments are given in Table 1, along with the parameter eigenvalues of rare earth elements. Comparative samples included those from the Chinese Loess Plateau loess (Chen et al., 1996; Ferrat et al., 2011; Zhang et al., 2018), Zhaosu loess (Jia, 2014), Wuwei loess (Zhang H et al., 1997), Badain Jaran Desert (Ferrat et al., 2011; Zhang et al., 2018), Qaidam Desert (Ferrat et al., 2011; Ling et al., 2018; Zhang et al., 2018), Taklimakan Desert (Ferrat et al., 2011; Zhang et al., 2018) and Tengger Desert (Ferrat et al., 2011; Zhang et al., 2018).

The content characteristics of rare earth elements

From Figure 4 and Table 1, the ΣREE values ranged from 139.02 to 185.47 $\mu g/g$, with an average value of 157.11 $\mu g/g$. Among the rare earth elements, the content of the Ce element was the largest (mean 66.4 $\mu g/g$), and the average range of the Lu element was the smallest (mean 0.34 $\mu g/g$), the contents of each rare earth elements from the largest to the smallest were as follows: Ce, La, Nd, Pr, Sm, Gd, Dy, Yb, Er, Eu, Ho, Tb, Tm, and Lu. The abundance order of rare earth elements in the YHC profile is almost the same as that of the UCC and other loess and desert, indicating that the stability of the rare earth elements was high. LREE values varied between 124.18 and 165.78 $\mu g/g$, with an average value of 140.67 $\mu g/g$. The HREE values varied from 14.69 to 19.69 $\mu g/g$, with an average value of 16.44 $\mu g/g$. The average ΣREE , LREE, and HREE values were close to those of the Chinese Loess Plateau loess and Tengger Desert, higher than those of UCC, and lower than those of other loess and deserts in this study.

In the various YHC profile layers, the content characteristics of the rare earth elements showed similarities and differences. The predominant commonality is the abundance order of the rare earth elements, demonstrating that the provenance of the YHC profile was relatively consistent. As shown in Figures 7A–C, ΣREE , LREE, and HREE exhibited similar depth-based variations, which were distinct in different layers, with higher values in the paleosol samples and lower values in the loess horizon samples. This suggests that rare earth

elements can serve as a record of stratigraphic changes to some extent; however, at 380–350 cm of the L1 layer, all three curves exhibited a notable peak that may be attributable to the contribution of additional sources.

Rare earth elements partitioning mode

The standardized partition curves are comprehensive reflections of the geochemical characteristics of the rare earth elements. According to the normalized rare earth elements distribution model diagram of chondrite (Figures 5A–F), the distribution curves of different layers in the Menyuan Basin closely coincided with each other, displaying prominent right-leaning L-shaped curves with steep La–Eu and gentle Gd–Lu parts, which were relatively enriched in LREE and deficient in HREE, respectively. The La, Ce, and Pr contents were higher, contributing to the relative enrichment of LREE. The normalized curves for all samples reveal a V-shape at Eu, indicating an apparent negative Eu anomaly, but no discernible change at Ce, indicating a weak Ce anomaly. The high consistency of the distribution curves among samples in diverse strata suggests that rare Earth fractionation of the YHC profile sediments is synchronous. After chondrite normalization, the rare earth elements distribution curves of loess sediments in various areas were nearly parallel to the YHC profile with similar morphology, exhibiting a right-sloping characteristic (Figure 6A). All of them are enriched in LREE relative to HREE, with an apparent negative Eu anomaly and no obvious Ce anomaly, indicating that YHC sediments have a terrigenous origin and source regions similar to those previously stated.

The variation range of the normalized rare earth elements distribution curves in different layers is illustrated by a spidergram normalized to the UCC in Figures 5G–L; however, the distribution curves of the mean values are still nearly identical. LREE and HREE were both enriched relative to UCC, with HREE being more evident than LREE, which demonstrates that the sedimentary properties of the whole section were similar and that only individual samples differed. The distribution of all sediments on the UCC normalized curves exhibited a class linear distribution with considerable variations (Figure 6B). HREE enrichments were more significant than LREE enrichment, showing that the rare Earth element compositions of all sediments were similar to those of the UCC; however, the fractionation of rare earth elements in sediments from different locations varied, which may be related to the provenance and environment.

Eigenvalues of rare earth elements parameters

All the characteristic rare earth elements parameter values for the YHC profile are shown in Figure 7 and Table 1. The average weight of δCe is 1.02, fluctuating from 0.95 to 1.07, and most of the samples have no apparent anomalies and only a few samples in the upper L1, LT, and S0 layers exhibited positive anomalous δCe values (Figure 7I), indicating that the overall weathering loam formation conditions were poor during the deposition process, and no pronounced redox effect occurred. The δEu ranged from 0.55 to 0.84, with a mean value of 0.65, and all samples showed considerable negative anomalies (Figure 7H). The δEu fluctuations in each stratum were small, signifying that the

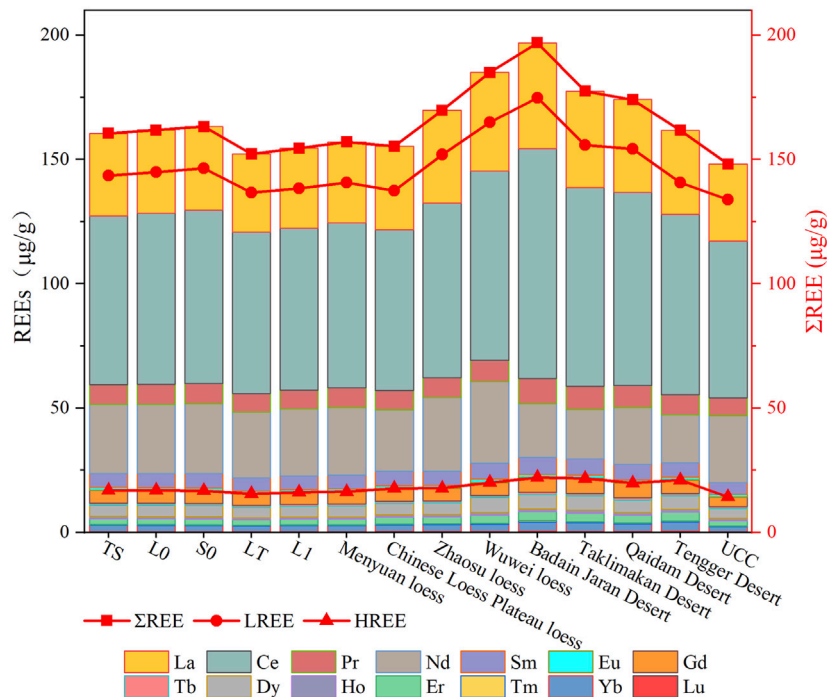


FIGURE 4

Comparison diagram of the contents of each rare Earth element in samples from different strata in the YHC profile and other areas.

comprehensive source of material in the YHC profile was relatively stable during deposition. The considerable δCe variation in the upper part of the L1 and LT layers reflects considerable climate change at that time and the possible input of other sources during the deposition of this formation.

The mean value of LREE/HREE was 8.57 (Figure 7D), varying between 7.91 and 9.35, near Wuwei and Zhaosu loess (Zhang H et al., 1997; Jia, 2014). The degree of differentiation was most substantial in the S0 stage, followed by the LT and TS stages, and was lowest in the LO and L1 stages. The trends of $(\text{La}/\text{Yb})_N$ and LREE/HREE were consistent (Figure 7E), showing fewer fractionations of rare earth elements in loess than in the paleosol.

$(\text{La}/\text{Sm})_N$ ranged from 3.61 to 4.11, with a mean value of 3.84 (Figure 7F). The contrast between the various horizons was inconspicuous, but the LREE was more enriched in the paleosol layer than in the loess layer. The mean value of $(\text{Gd}/\text{Yb})_N$ was 1.69, and the overall variation was insignificant (Figure 7G). There were three peaks, that is, in the upper part of L1, the junction of the LT and S0 layers, and the ground surface layer, indicating that HREEs were more deficient in these three depositional stages.

Overall, comparing the various rare earth elements parameters in the sediments from different layers of the YHC profile indicates that the overall changes in the Menyuan loess were negligible, and the rare earth elements parameters may not be sensitive indicators of climate change.

Discussion

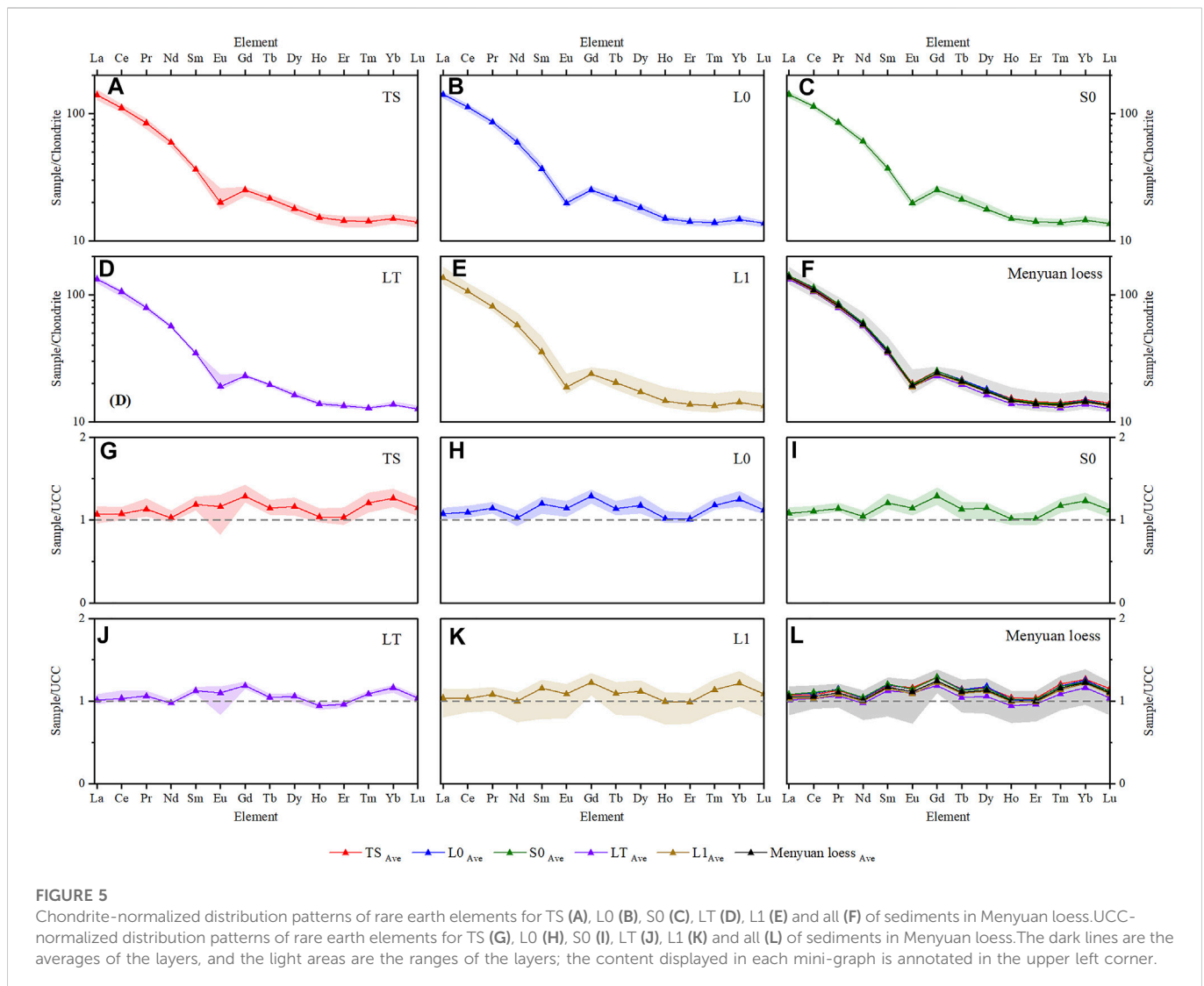
The composition of rare earth elements in sedimentary deposits is predominantly a combination of numerous environmental factors,

including source rocks, chemical weathering, and grain size composition (Ferrat et al., 2011; Casse et al., 2019; Thorpe et al., 2019; Li et al., 2021). Assessing the effects of chemical weathering and grain size composition on rare Earth element composition is necessary for establishing provenance discrimination with rare earth elements.

Chemical weathering on rare earth elements behaviours

Chemical weathering influences the abundance and behavior of rare earth elements (Casse et al., 2019). Clay minerals, one of the major host minerals of rare earth elements, are created in large quantities during chemical weathering, affecting the enrichment and migration of rare earth elements (Yang et al., 2019; Andrade et al., 2022).

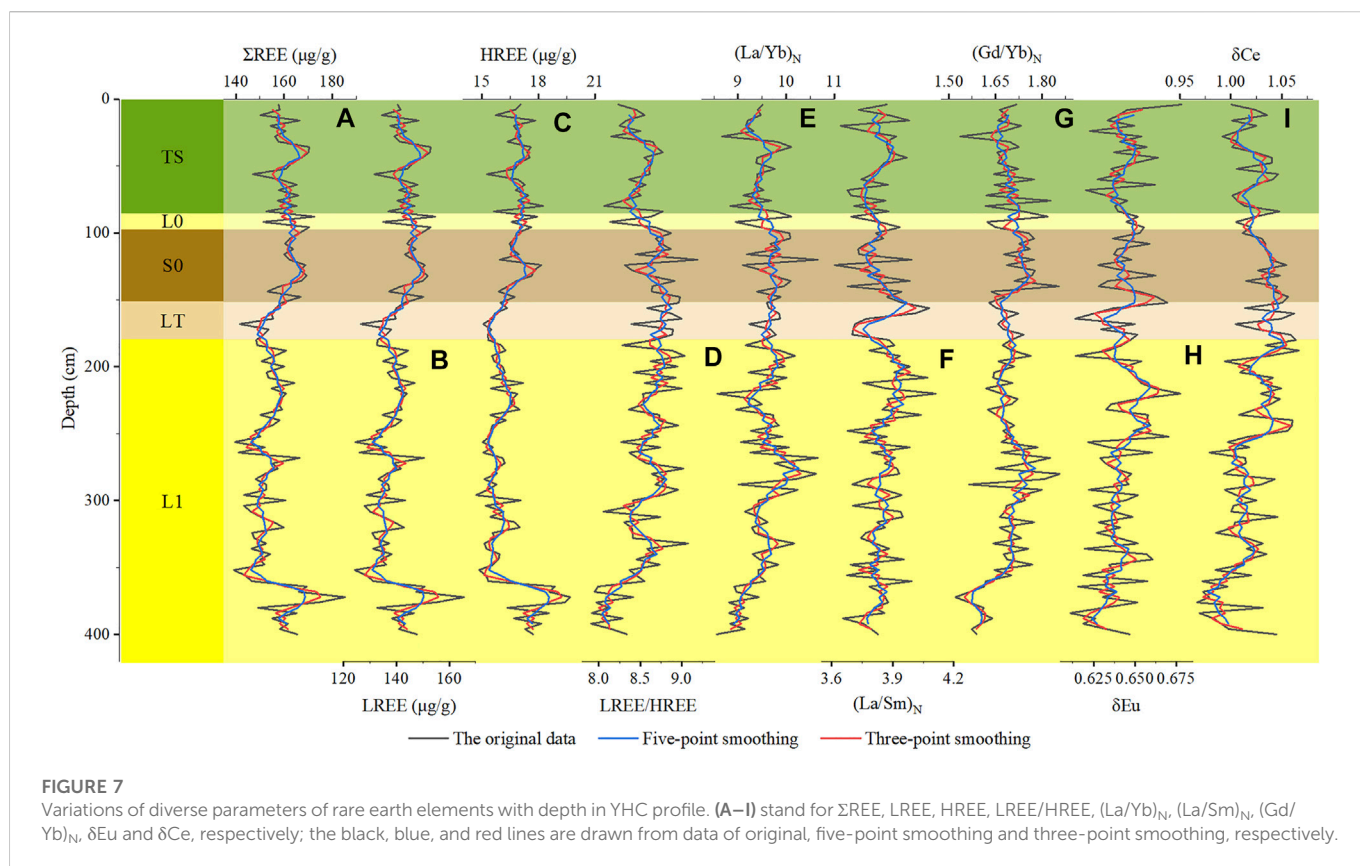
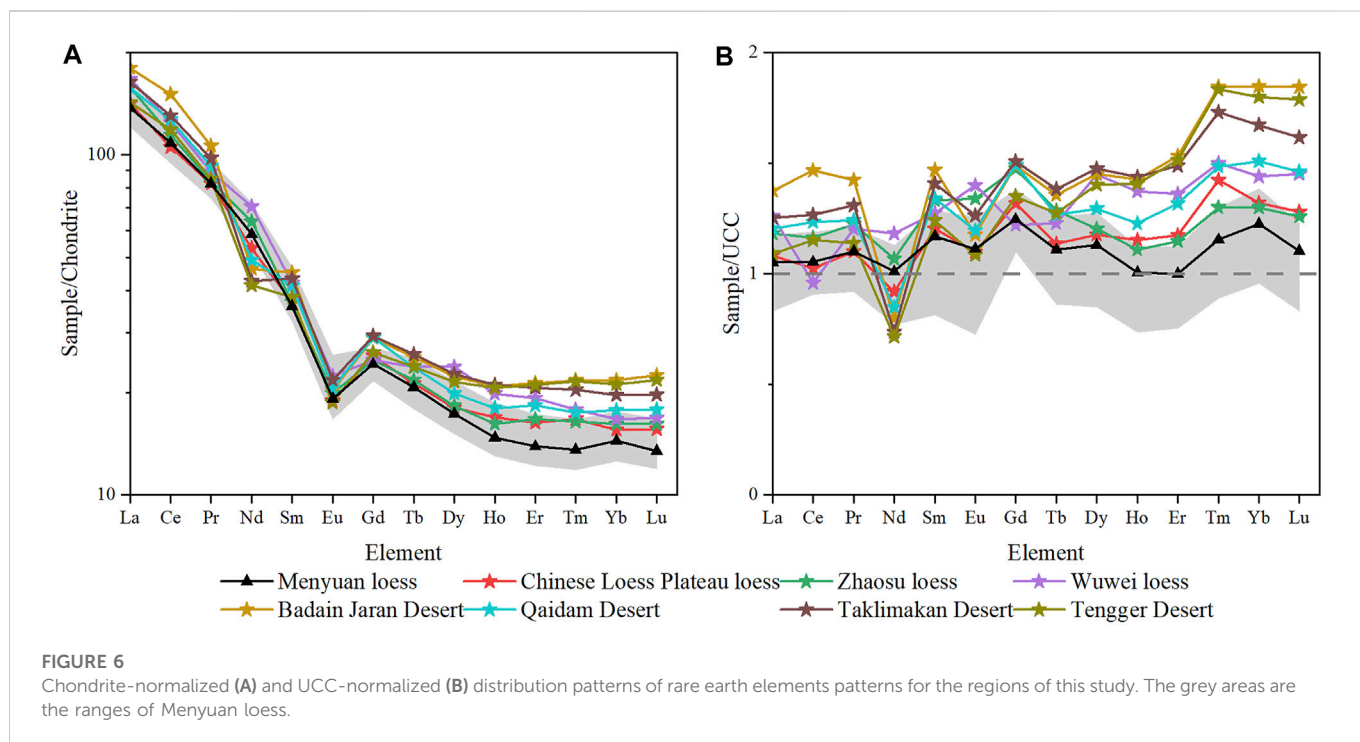
Paleosol layers are formed under warmer and wetter climatic conditions with substantial chemical weathering, and loess is included in drier and colder climatic conditions with weak chemical weathering (Skurzyński et al., 2020). The Chemical Index of Alteration (CIA, $(\text{Al}_2\text{O}_3/(\text{Al}_2\text{O}_3 + \text{CaO}^* + \text{Na}_2\text{O} + \text{K}_2\text{O})) \times 100$ (molar ratio)) is a vital indicator of the intensity of chemical weathering and is frequently employed in various sediments (Nesbitt and Young, 1982; Wang G et al., 2020; Deng et al., 2022b). The variation of CIA in the YHC profile (in submission, Figure 8A) shows that the CIA varies markedly with stratigraphy, with the highest CIA values in the paleosol layer and the lowest CIA values in the loess layer, clearly showing the variation in chemical weathering processes at different stages. The total CIA values for the YHC profile were slightly lower, indicating that the Menyuan loess experienced weak chemical weathering under an arid climate and low precipitation.



The properties of the rare earth elements resulted in the abundance of Σ REE and LREE of the paleosol being more significant than that of the loess in the YHC profile. During the formation of the paleosol, the warm and humid climatic conditions enhanced the mobility of the rare earth elements, and the active rare earth elements were enriched and preserved by simultaneously composing complex ions linked to other stable matter in the form of hydroxyl or heteronuclear multiple complex associations. This resulted in intense leaching of carbonate, which led to the relative enrichment of the rare earth elements component (Zhang et al., 2009; Andrade et al., 2022). Minor differences exist between the loess and paleosol in the Menyuan Basin, reflecting poor pedogenesis by weathering in the survey region. The δ Ce indicator also reflects the same results, which are consistent with the conclusions of the CIA. Owing to their diverse properties, LREEs and HREEs behave differently under chemical weathering within the rare earth elements. When chemical weathering is more substantial, HREEs are more likely to form bicarbonates in solution than LREEs and preferentially dissolve and migrate, while clays preferentially adsorb LREEs. The LREEs and HREEs undergo fractionation, resulting in a relative enrichment of LREEs and a relative loss of HREEs (Ma et al., 2007; Laveuf and Cornu, 2009; Chapela Lara et al., 2018; Andrade

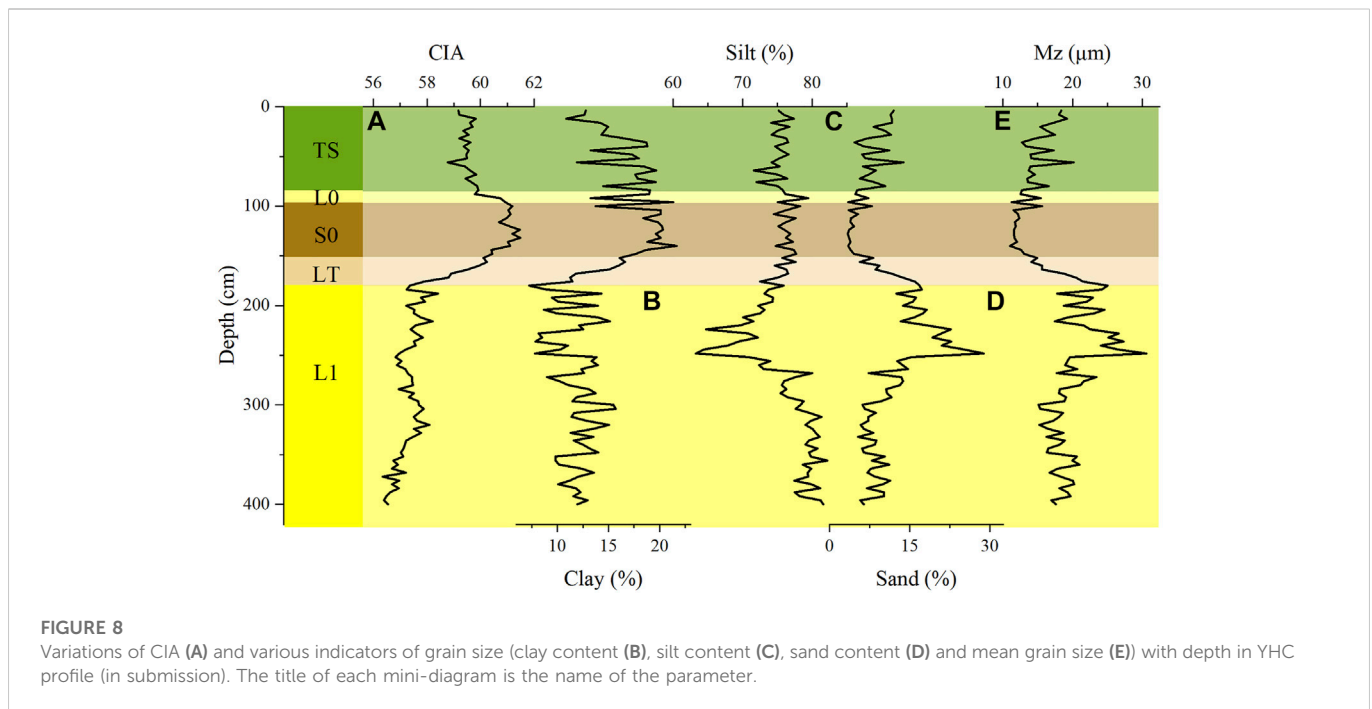
et al., 2022). The LREEs and HREEs fractionation of the paleosol layer is higher than that of the loess layer in the YHC profile, indicating that the paleosol layer suffered more substantial chemical weathering, the CIA curve in Figure 8A also confirms that the paleosol layer was subjected to more intense chemical weathering. Notably, the HREE abundance of the paleosol was greater than that of the loess in the YHC profile, which may be caused by the dilution effect of carbonate in the loess layer (Chen et al., 2017); however, specific carbonate data were lacking for interpretation, and further analysis is required through tests such as leaching and carbonate content determination. The results for LREE/HREE and $(La/Yb)_N$ in the YHC profile are consistent with common sense. $(La/Sm)_N$ and $(Gd/Yb)_N$ further reflect the internal fractionation of LREEs and HREEs, respectively; the former varies insignificantly and the latter varies at markedly higher values in the paleosol layers in the YHC profile. LREEs are not susceptible to HREE activation by chemical weathering; therefore, the internal fractionation of LREEs is insensitive to the response of weathering intensity compared with HREEs (Chapela Lara et al., 2018).

Although most rare Earth element indices can reflect the difference between the loess and paleosol layers, and there are positive correlations between these indices and CIA in the YHC



profile, the correlation coefficients were extremely low (Figure 9), which indicated that the rare earth elements were somewhat indicative of weathering intensity; however, they were insensitive to chemical

weathering and climate change in the Menyuan loess, and further elucidation of these rare earth elements indices is not suitable as an index of chemical weathering intensity in this area. The relationship



between these rare earth elements indices and chemical weathering implies that rare-earth-element-controlling behavior is not chemical weathering intensity in the Menyuan Basin. The reason for limiting the ability of rare Earth element indices may be the arid climate and minimal precipitation in the region, where the weathering process is dominated by physical weathering, and chemical weathering is weak and restricted. Numerous studies in other arid and semi-arid areas have shown that aeolian sediments are in the early stages of weathering, and that the degree of weathering is generally low (Li et al., 2016; Li et al., 2021; Xu et al., 2022).

Overall, the impact of chemical weathering on the behavior of rare earth elements in Menyuan loess is negligible.

Effect of grain size composition on rare earth elements behaviours

Grain size is one of the most fundamental physicochemical properties of sediments, holding information about provenance, transport, and weathering, and it has a substantial influence on other sedimentary characteristics, such as magnetic susceptibility and rare Earth element abundances (Li et al., 2021; Shi et al., 2021). As the fine grain size fraction contains a large host of rare earth elements, the rare earth elements abundance generally correlates well with the clay content, which means that rare earth elements tend to be enriched in fine grain size and deficient in coarse grain size; therefore, the grain size of the sediment can influence the content and distribution of rare earth elements (Taylor and McLennan, 1985). However, it has been shown that grain size has no substantial effect on rare earth elements (Ferrat et al., 2011; Zhang et al., 2018). Assessing the relationship between rare earth elements and grain-size indicators for loess in the study area is crucial to probe the provenance of the Menyuan loess with rare earth elements abundances and parameters.

The grain size results of the YHC profile show that its mean grain size (M_z) ranges from 11.02 to 30.62 μm , with a mean value of 17.63 μm , and is dominated by silt with a content ranging from 61.64% to 82.21%. Furthermore, the clay content ranges from 7.11% to 21.68% and sand content ranges from 3.42% to 28.87% (in submission, Figures 8B–E). The grain size indicators of the various horizons contrast substantially, but the distribution patterns of rare earth elements are relatively consistent across the different horizons (Figure 5), suggesting that the rare earth elements distribution patterns are independent of grain size and that grain size has no significant effect on rare earth elements in the Menyuan loess. To further explore the influence of grain size on rare earth elements, this study linked the grain size parameter with the rare earth elements parameters (Figure 10). According to Figure 10, ΣREE , LREE, and HREE exhibit a significant positive correlation with clay content and a remarkable negative correlation with sand content and M_z . There is a characteristic that the abundance of rare earth elements in the Menyuan loess gradually decreases with the coarsening of sediment grain size, which is consistent with the trend of enrichment of rare earth elements to the fine-grained fraction, as suggested by previous authors (Taylor and McLennan, 1985). Rare earth elements enter the lattice of clay minerals by isomorphism or are preferentially concentrated in the fine-grained fraction due to adsorption onto ultra-abrasive heavy minerals such as zircon, rutile, and monazite. In contrast, the dilution of quartz, carbonate, and other rock-forming minerals in coarse-grained sediments increases the parasitifer content of non-rare-earth-elements while decreasing the clay mineral content, which is unfavorable for rare earth elements enrichment (Caggianelli et al., 1992; Mongelli, 1995; Hao et al., 2010; Hu and Yang, 2016; Chen et al., 2017; Du et al., 2018; Li et al., 2021). This further explains why the paleosol layer with a higher clay content than the loess layer with a higher sand content has a greater abundance of rare earth elements. Two other points should be noted: firstly, the correlation coefficients of the grain size parameters with ΣREE and LREE are consistent and

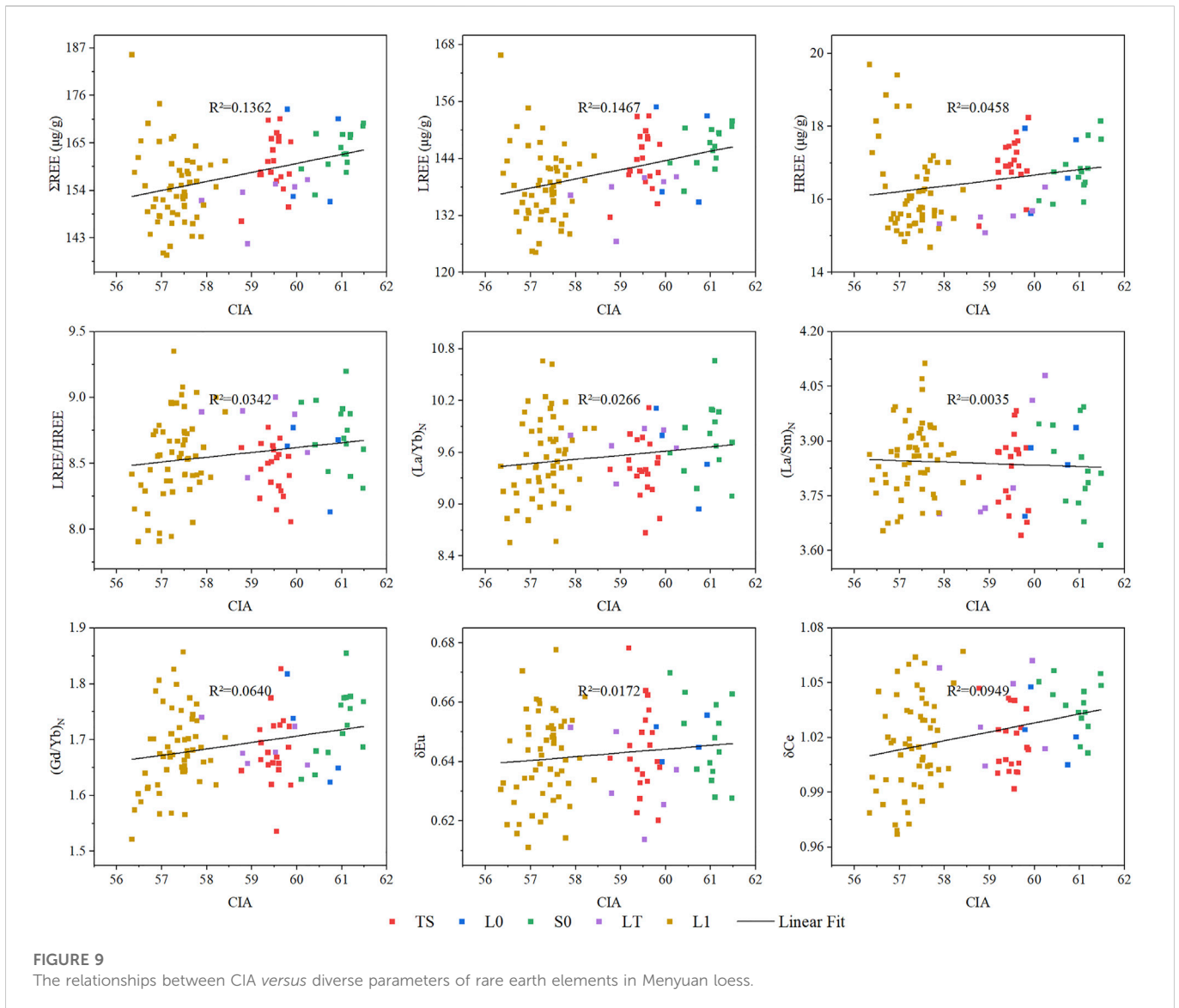


FIGURE 9
The relationships between CIA versus diverse parameters of rare earth elements in Menyuan loess.

higher than those with HREE, indicating ΣREE and LREE are more closely related and HREE is more active than LREE; secondly, the abundance of rare earth elements is not significantly related to the main component of loess (silt content), and the correlation coefficients with other grain size indicators are less than 0.5 (at the 0.01 level), showing extremely weak correlations and indicating grain size composition has little influence on the rare earth elements abundance in Menyuan loess.

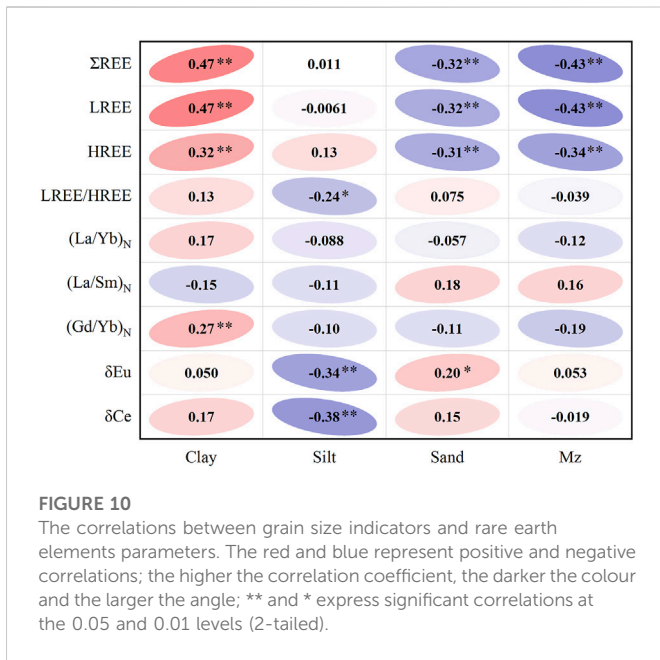
Figure 10 also shows that the correlation coefficients between the characteristic indices of rare earth elements and grain size parameters are all less than 0.38 with extremely weak correlations, the majority of which were less than 0.2 and did not pass the significance test, denoting that the grain size of Menyuan loess has minimal constraints on the characteristic indices and fractionation of rare earth elements, as is also the case in some deserts of northwestern China (Du et al., 2018; Li et al., 2021). Notably, δCe and (La/Sm)_N tend to be enriched in the fine-grained fraction owing to clay mineral adsorption (Nesbitt, 1979; Braun et al., 1990). In the YHC profile, only δCe was positively correlated with clay content, whereas (La/Sm)_N was negatively correlated; both correlations were quite low. It can be

concluded that δCe and (La/Sm)_N in the Menyuan loess were not significantly influenced by grain size parameters. The findings of Du et al. (2018); Li et al. (2021) also demonstrate that δCe and (La/Sm)_N are minimally affected by grain size in arid zones, such as the Qaidam Desert and Badain Jaran Desert, and may be used as proxies for determining the source of aeolian sediments.

The abundance, distribution pattern, and characteristic indices of rare earth elements in the Menyuan loess were minimally governed by particle size at the visible scale.

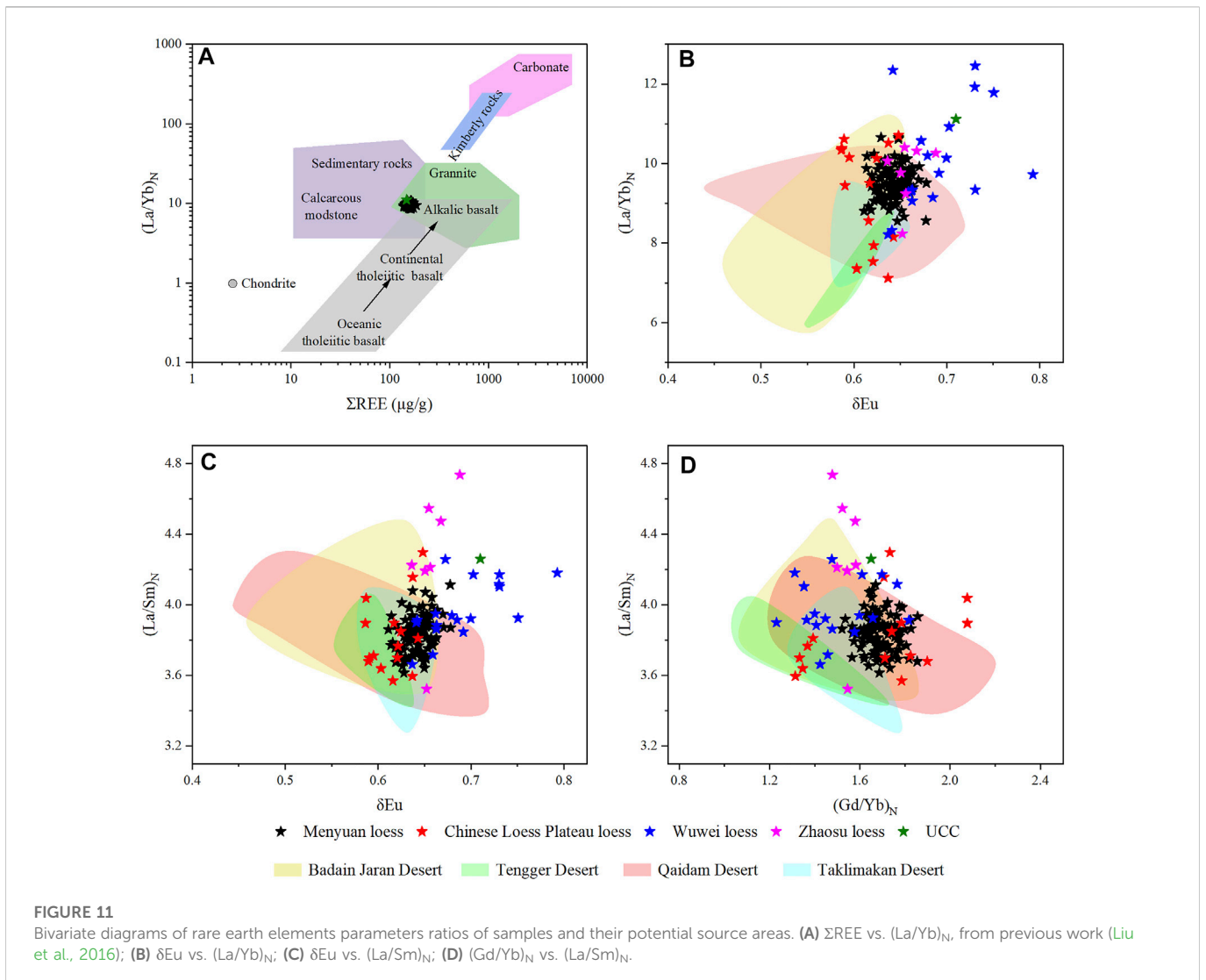
Supply of provenance in Menyuan Loess

The rare earth elements parameters are a function of provenance information, chemical weathering, and grain size composition, and the effects of weathering and grain size on rare earth elements in the Menyuan loess are insignificant. Thus, the dominant factor was the influence of the source rock composition on the characteristic parameters and partitioning patterns of rare earth elements in the research region.



Provenance information carried by other parameter ratios such as $(La/Yb)_N$, δEu , $(La/Sm)_N$, and $(Gd/Yb)_N$ in the Munyuan loess was retained. Many comprehensive investigations have shown a functional relationship between ΣREE and $(La/Yb)_N$, with $(La/Yb)_N$ increasing with ΣREE and distinct projection zones for various rocks, which may be utilized to establish source rock properties (Zhang et al., 2009; Liu et al., 2016). In the ΣREE vs. $(La/Yb)_N$ plot (Figure 11A), most of the samples were concentrated in overlapping areas of granite, alkaline basalt, and sedimentary rocks, indicating that the source of the Munyuan loess is very complicated. The granites contained a relatively high concentration of rare earth elements, being enriched in LREE, having high LREE/HREE ratios, and exhibiting significant negative Eu anomalies. In contrast, the basal basalts were relatively low in rare earth elements and moderately increased in HREE, with low LREE/HERR ratios and minor Eu anomalies (Cullers and Graf, 1984; Condie, 1993; Hai et al., 2021). The Menyuan loess has low rare earth elements and HREE contents, high LREE/HREE ratios, and substantial negative Eu anomalies; hence, it is doubtful that the Menyuan loess source rocks are basaltic, but rather granite and sedimentary rocks.

In this study, the commonly employed δEu vs. $(La/Yb)_N$, δEu vs. $(La/Sm)_N$, and (La/Sm) vs. $(La/Gd)_N$ variograms were selected to



analyze the material source areas of the Menyuan loess (Reichow et al., 2005; Wei et al., 2018). Figures 11B–D shows that the Menyuan loess data are all relatively concentrated, indicating that its source is reasonably consistent and has not altered significantly. When comparing the loess data from other regions, there is considerable overlap between the Menyuan and Zhaosu loess, a substantial overlap with the Chinese Loess Plateau loess, and a less overlap with the Wuwei loess. There is some correlation between the loess sources in the arid and semi-arid regions of northwest China, with the Menyuan loess being less correlated with the closer Wuwei loess but more correlated with the more distant Zhaosu loess. This suggests that the Menyuan Basin has largely received foreign aeolian deposits. The material source of the Zhaosu loess is mainly the deserts of arid Central Asia (Song et al., 2014); the Badain Jaran Desert, the Qaidam Desert, and the Taklimakan Desert are considered to be the material source areas of the loess on the Chinese Loess Plateau (Sun, 2002; Zhang et al., 2003; Sun et al., 2020); and the Tengger Desert is the source of Wuwei loess (Zhang H et al., 1997). The potential material source areas of the Menyuan loess are probably related to the loess's provenance in the aforementioned places. By comparing the data on potential source areas around the Menyuan loess, it is evident that all the points of the YHC profile fall within the Qaidam Desert region, with the majority of issues falling within the Badain Jaran Desert and a small proportion projected within the Taklimakan Desert and Tengger Desert, suggesting that the Menyuan loess is not derived from a single desert and that multiple source areas may exist. Some fluvial and ice-water deposits within the Menyuan Basin may also be a potential source of Menyuan loess. Due to the lack of rare earth elements data for these deposits, we do not elaborate too much in this study and intend to investigate them with other means in subsequent reports. Through evidence of rare earth elements, the Qaidam Desert and Badain Jaran Desert are the main source areas, and the Taklimakan Desert and Tengger Desert are the secondary source areas, due to wind and topography.

Wind was the main driving factor behind the NETP loess formation (Stauch et al., 2012). The NETP is predominantly influenced by westerly and Asian monsoons, in which both the westerly and winter winds are crucial dust transport drivers (Ferrat et al., 2011; Stauch et al., 2012; Wei et al., 2018; Zhang et al., 2018). Loess is a product of dry and cold periods, and prior research (An et al., 2012) has shown that westerly circulation predominantly influenced the NETP during the Last Glacial Period. During the glacial epoch, especially after MIS3, reduced solar radiation in the northern hemisphere at high latitudes in summer and lower temperatures in the Greenland region and the North Atlantic sea surface inhibited the evaporation of seawater, resulting in less water vapor being carried by westerly winds and triggering a relatively dry climate across the westerly zone (Dansgaard et al., 1993; Ding et al., 1995; Alley et al., 2010; Moreno Chamorro et al., 2020; Chen and Liu, 2022). The expansion of the Eurasian ice cap, blowing of cold air over the ice cap to the mid-latitudes, intensification of the Siberian–Inner Mongolian high pressure, strong winter winds blocking warm and humid air masses from penetrating inland, intensification of airflows and the reduction of precipitation in the arid and semi-arid regions of Asia, and evolution of the environment in a colder and drier direction (Ding et al., 1995; Dykoski et al., 2005; Chen and Liu, 2022). Environmental degradation leads to reduced vegetation in the source area and increased material exported from the desert or Gobi (Zhang X. Y et al., 1997; Jia et al., 2020; Kang et al., 2022). The westerly winds

prevail year-round over the NETP, and the Menyuan Basin is positioned downwind of the Qaidam and Taklimakan Deserts.

Large quantities of dust are emitted from the two source areas, and the dust then rises to the upper air by surface winds and is transported with westerly winds to the Chinese Loess Plateau and other eastern Asian areas where it accumulates and forms thick loess (Goudie and Middleton, 2006). The Menyuan Basin is a station on the virtual channel for dust transport from the deserts of arid Central Asia to Eastern Asia; therefore, a portion of the dustfall will also settle in the Menyuan Basin, which is confirmed by dustfall in ice cores on the Qilian Mountains (Wei et al., 2018). Geographically, the Menyuan Basin is located near the Badangilin Desert and the Tengger Desert. Strong winter winds are expected to transport these dust particles to the Menyuan Basin from these two deserts, releasing a significant amount of dust into the surrounding areas *via* cold frontal channels in winter and spring (Goudie and Middleton, 2006). Indicators of rare earth elements indicate that the more distant Batangilin Desert, rather than the adjacent Tengger Desert, and provides more material for the Menyuan Loess. The results (An et al., 2012; Xie et al., 2019; Li Y et al., 2022) show that the NETP is frequently exposed to northwesterly and northerly winds and rarely to northeasterly winds in winter; therefore, the Menyuan Basin should receive dust from the Batangilin Desert in the north more efficiently, and material from the Tengger Desert in the northeast can only be transported to the Menyuan Basin during extreme dust storm conditions. In addition to the wind force, topography also has a significant influence (Liang et al., 2022). The Menyuan Basin is an enclosed terrain surrounded by tall mountains that become natural barriers to resist coarse-grained material carried by near-surface winds from the surrounding source areas. This results in the Tengger Desert, the closest source area to the study area, not being the main source area for the Menyuan loess, which is more likely to be formed by the transport of delicate particulate matter by high-altitude air currents.

The indicators of the YHC profile have increased our understanding of aeolian sediment accumulation processes and portrayed a crucial pathway for dust transfer from arid Central Asia to the east. Previous studies on the paleodust transport process and loess accumulation on the Chinese Loess Plateau and arid Central Asia have been relatively comprehensive, but research on the loess in the NETP is lacking, so more systematic research work on the Tibetan Plateau is required to provide a complete picture of the accumulation pattern of loess at different times and spaces.

Conclusion

In this study, a systematic geochemical investigation of rare earth elements was conducted on the YHC loess-paleosol profile of the Menyuan Basin. The following conclusions were obtained by analyzing the indicators and distribution characteristics of rare earth elements in the Menyuan loess.

- 1) The indices and distribution curves of rare earth elements in the diverse strata of the YHC profile did not differ significantly, with only minor deviations in the paleosol and loess. The Menyuan loess is extremely comparable to the loess in other locations of northwestern China, with negative slopes in the distribution curves, steeper La-Eu curves, and gentler Gd-Lu curves, showing relative enrichment of LREE and relative loss of HREE, apparent Eu negative anomalies, and no apparent Ce anomalies, revealing a general association with the loess in arid northwestern China.

- 2) The correlations between various rare Earth element parameters and chemical weathering, and grain size composition were extremely low in the Menyuan loess. The influence of chemical weathering and particle diameter on rare Earth element in the loess of the study area is minimal, indicating that rare Earth element parameters contain a wealth of information regarding the content source, and indicators such as $(La/Yb)_N$, δEu , $(La/Sm)_N$, and $(Gd/Yb)_N$ are more suitable for determining the source of dust.
- 3) According to the source discrimination diagrams of ΣREE and $(La/Yb)_N$, the Menyuan loess was mostly derived from a mixed source rock consisting of granite and sedimentary rocks. A comparison of the $(La/Yb)_N$, δEu , $(La/Sm)_N$, and $(Gd/Yb)_N$ parameters of potential source areas shows that arid Central Asia, dominated by the Qaidam Desert and Taklimakan Desert, is the primary source area of Menyuan loess, and dust particles released from these deserts are transported to the Menyuan Basin by the Westerlies and deposited to form loess. In addition, the Badain Jaran Desert is also an essential source of material for the Menyuan loess by winter winds, and some Tengger Desert materials are also transported to the Menyuan Basin by winter winds, but the material transported from the Tengger Desert has a negligible contribution.

Data availability statement

The original contributions presented in the study are included in the article/Supplementary Material, further inquiries can be directed to the corresponding author.

Author contributions

YS: designed the study, formal analysis, investigation, writing, and editing. CE: conceptualization, funding acquisition, investigation, and writing. QP and ZZ: investigation and writing. JZ: investigation and formal analysis. WY and CX: experimental treatment and formal analysis.

References

- Alley, R. B., Andrews, J. T., Brigham-Grette, J., Clarke, G. K. C., Cuffey, K. M., Fitzpatrick, J. J., et al. (2010). History of the Greenland ice sheet: Paleoclimatic insights. *Quat. Sci. Rev.* 29, 1728–1756. doi:10.1016/j.quascirev.2010.02.007
- An, Z., Kukla, G. J., Porter, S. C., and Xiao, J. (1991). Magnetic susceptibility evidence of monsoon variation on the Loess Plateau of central China during the last 130, 000 years. *Quat. Res.* 36, 29–36. doi:10.1016/0033-5894(91)90015-W
- An, Z., Colman, S. M., Zhou, W., Li, X., Brown, E. T., Jull, A. J. T., et al. (2012). Interplay between the Westerlies and asian monsoon recorded in lake Qinghai sediments since 32 ka. *Sci. Rep.* 2, 619. doi:10.1038/srep00619
- Andrade, G. R. P., Cuadros, J., Barbosa, J. M. P., and Vidal-Torrado, P. (2022). Clay minerals control rare earth elements (REE) fractionation in Brazilian mangrove soils. *CATENA* 209, 105855. doi:10.1016/j.catena.2021.105855
- A. S. Goudie and N. J. Middleton (Editors) (2006). "Dust entrainment, transport and deposition." *Desert dust in the global system* (Berlin, Heidelberg: Springer Berlin Heidelberg), 13–31. doi:10.1007/3-540-32355-4_2
- Börker, J., Hartmann, J., Amann, T., and Romero-Mujalli, G. (2018). Terrestrial sediments of the earth: Development of a global unconsolidated sediments map database (GUM). *Geochem. Geophys. Geosystems* 19 (4), 997–1024. doi:10.1002/2017gc007273
- Braun, J.-J., Pagel, M., Muller, J.-P., Bilong, P., Michard, A., and Guillet, B. (1990). Cerium anomalies in lateritic profiles. *Geochimica Cosmochimica Acta* 54, 781–795. doi:10.1016/0016-7037(90)90373-S
- Caggianelli, A., Fiore, S., Mongelli, G., and Salvemini, A. (1992). REE distribution in the clay fraction of pelites from the southern Apennines, Italy. *Chem. Geol.* 99, 253–263. doi:10.1016/0009-2541(92)90180-D
- Casse, M., Montero-Serrano, J.-C., St-Onge, G., and Poirier, A. (2019). REE distribution and Nd isotope composition of estuarine waters and bulk sediment leachates tracing lithogenic inputs in eastern Canada. *Mar. Chem.* 211, 117–130. doi:10.1016/j.marchem.2019.03.012
- Chapela Lara, M., Buss, H. L., and Pett-Ridge, J. C. (2018). The effects of lithology on trace element and REE behavior during tropical weathering. *Chem. Geol.* 500, 88–102. doi:10.1016/j.chemgeo.2018.09.024
- Chen, Y., and Liu, X. (2022). Vegetation and climate changes since the middle MIS 3 inferred from a Lake Ailike pollen record, xinjiang, arid central Asia. *Quat. Sci. Rev.* 290, 107636. doi:10.1016/j.quascirev.2022.107636
- Chen, J., Wang, H., and Lu, H. (1996). Behaviours of REE and other trace elements during pedological weathering—evidence from chemical leaching of loess and palaeosol from the luochuan section in central China. *Acta Geol. Sin. - Engl. Ed.* 9, 290–302. doi:10.1111/j.1755-6724.1996.mp9003006.x
- Chen, F., Wu, D., Chen, J., Zhou, A., Yu, J., Shen, J., et al. (2016). Holocene moisture and east Asian summer monsoon evolution in the northeastern Tibetan plateau recorded by lake Qinghai and its environs: A review of conflicting proxies. *Quat. Sci. Rev.* 154, 111–129. doi:10.1016/j.quascirev.2016.10.021
- Chen, X., Song, Y., Li, J., Fang, H., Li, Z., Liu, X., et al. (2017). Size-differentiated REE characteristics and environmental significance of aeolian sediments in the Ili Basin of Xinjiang, NW China. *J. Asian Earth Sci.* 143, 30–38. doi:10.1016/j.jseae.2017.03.030
- Chen, F., Chen, J., Huang, W., Chen, S., Huang, X., Jin, L., et al. (2019). Westerlies Asia and monsoonal Asia: Spatiotemporal differences in climate change and possible mechanisms on decadal to sub-orbital timescales. *Earth-Science Rev.* 192, 337–354. doi:10.1016/j.earscirev.2019.03.005

Funding

This work was jointly supported by the Natural Science Foundation of Qinghai Provincial Science and Technology Department (2021-ZJ-918), the National Natural Science Foundation of China (Nos. 41761042 and 41361047), and the Free Exploration Research Project of the Key Laboratory of Tibetan Plateau Land Surface Processes and Ecological Conservation (Ministry of Education) (TGEZT-2022-03).

Acknowledgments

The authors sincerely thank reviewers for their constructive comments and suggestions. We also thank editors, Joel Roskin and Noam Greenbaum, who were extremely helpful. We would like to thank Editage (www.editage.cn) for English language editing.

Conflict of interest

Author WY was employed by the company Qinghai Institute of Water Conservancy and Hydropower Research Co.

The remaining authors declare that the research was conducted in the absence of any commercial or financial relationships that could be construed as a potential conflict of interest.

Publisher's note

All claims expressed in this article are solely those of the authors and do not necessarily represent those of their affiliated organizations, or those of the publisher, the editors and the reviewers. Any product that may be evaluated in this article, or claim that may be made by its manufacturer, is not guaranteed or endorsed by the publisher.

- Chen, H., Chen, Z., Chen, Z., Chen, H., and Ou, X. (2021). Migration of rare earth elements in the topsoil of abandoned mines under rainfall leaching. *J. Radioanalytical Nucl. Chem.* 328, 1189–1198. doi:10.1007/s10967-021-07741-9
- Condie, K. C. (1993). Chemical composition and evolution of the upper continental crust: Contrasting results from surface samples and shales. *Chem. Geol.* 104, 1–37. doi:10.1016/0009-2541(93)90140-E
- Cullers, R. L., and Graf, J. L. (1984). “Chapter 7 - rare earth elements in igneous rocks of the continental crust: Predominantly basic and ultrabasic rocks,” in *Developments in geochemistry*. Editor P. Henderson (Netherlands: Elsevier), 237–274. doi:10.1016/B978-0-444-42148-7.50012-5
- Dansgaard, W., Johnsen, S. J., Clausen, H. B., Dahl-Jensen, D., Gundestrup, N. S., Hammer, C. U., et al. (1993). Evidence for general instability of past climate from a 250-kyr ice-core record. *Nature* 364, 218–220. doi:10.1038/364218a0
- Deng, K., Yang, S., Du, J., Lian, E., and Vance, D. (2022a). Dominance of benthic flux of REEs on continental shelves: Implications for oceanic budgets. *Geochem. Persp. Lett.* 22, 26–30. doi:10.7185/geochemlet.2223
- Deng, K., Yang, S., and Guo, Y. (2022b). A global temperature control of silicate weathering intensity. *Nat. Commun.* 13, 1781. doi:10.1038/s41467-022-29415-0
- Ding, Z., Liu, T., Rutter, N. W., Yu, Z., Guo, Z., and Zhu, R. (1995). Ice-volume forcing of east Asian winter monsoon variations in the past 800,000 years. *Quat. Res.* 44, 149–159. doi:10.1006/qres.1995.1059
- Ding, Z. L., Sun, J. M., Yang, S. L., and Liu, T. S. (2001). Geochemistry of the Pliocene red clay formation in the Chinese Loess Plateau and implications for its origin, source provenance and paleoclimate change. *Geochimica Cosmochimica Acta* 65, 901–913. doi:10.1016/S0016-7037(00)00571-8
- Du, S., Wu, Y., and Tan, L. (2018). Geochemical evidence for the provenance of aeolian deposits in the Qaidam Basin, Tibetan Plateau. *Aeolian Res.* 32, 60–70. doi:10.1016/j.aeolia.2018.01.005
- Dykoski, C., Edwards, R., Cheng, H., Yuan, D., Cai, Y., Zhang, M., et al. (2005). A high-resolution, absolute-dated Holocene and deglacial Asian monsoon record from Dongge Cave, China. *Earth Planet. Sci. Lett.* 233, 71–86. doi:10.1016/j.epsl.2005.01.036
- E, C., Lai, Z., Sun, Y., Hou, G., Yu, L., and Wu, C. (2012). A luminescence dating study of loess deposits from the Yili River basin in Western China. *Quat. Geochronol.* 10, 50–55. doi:10.1016/j.quageo.2012.04.022
- E, C., Sohbaty, R., Murray, A. S., Buylaert, J.-P., Liu, X., Yang, L., et al. (2018). Hebei loess section in the anyemaqen mountains, northeast Tibetan plateau: A high-resolution luminescence chronology. *Boreas* 47, 1170–1183. doi:10.1111/bor.12321
- Ferrat, M., Weiss, D. J., Strekopytov, S., Dong, S., Chen, H., Najorka, J., et al. (2011). Improved provenance tracing of Asian dust sources using rare earth elements and selected trace elements for palaeomonsoon studies on the eastern Tibetan Plateau. *Geochimica Cosmochimica Acta* 75, 6374–6399. doi:10.1016/j.gca.2011.08.025
- Gallelo, G., Ramacciotti, M., García-Puchol, O., Chenery, S., Cortell-Nicolau, A., Cervera, Mar. L., et al. (2021). Analysis of stratigraphical sequences at Cocina Cave (Spain) using rare earth elements geochemistry. *Boreas* 50, 1190–1208. doi:10.1111/bor.12530
- Hai, L., Xu, Q., Mu, C., Tao, R., Wang, L., Bai, J., et al. (2021). Geochemical characteristics and geologic significance of rare earth elements in oil shale of the Yan'an Formation in the Tanshan area, in the Liupanshan Basin, China. *Interpretation* 9, T843–T854. doi:10.1190/INT-2020-0232.1
- Hao, Q., Guo, Z., Qiao, Y., Xu, B., and Oldfield, F. (2010). Geochemical evidence for the provenance of middle Pleistocene loess deposits in southern China. *Quat. Sci. Rev.* 29, 3317–3326. doi:10.1016/j.quascirev.2010.08.004
- Heller, F., and Liu, T. (1984). Magnetism of Chinese loess deposits. *Geophys. J. Int.* 77, 125–141. doi:10.1111/j.1365-246X.1984.tb01928.x
- P. Henderson (Editor) (1984). *Rare earth element geochemistry* (Amsterdam ; New York: Elsevier).
- Hu, F., and Yang, X. (2016). Geochemical and geomorphological evidence for the provenance of aeolian deposits in the Badain Jaran Desert, northwestern China. *Quat. Sci. Rev.* 131, 179–192. doi:10.1016/j.quascirev.2015.10.039
- Inguaggiato, C., Burbano, V., Rouwet, D., and Garzón, G. (2017). Geochemical processes assessed by Rare Earth Elements fractionation at “Laguna Verde” acidic-sulphate crater lake (Azufra volcano, Colombia). *Appl. Geochem.* 79, 65–74. doi:10.1016/j.apgeochem.2017.02.013
- Jia, H., Wu, J., Zhang, H., and Yi, S. (2020). Pollen-based climate reconstruction from Ebi Lake in northwestern China, Central Asia, over the past 37,000 years. *Quat. Int.* 544, 96–103. doi:10.1016/j.quaint.2020.02.033
- Jia, L. (2014). *Rare earth elements characteristics aeolian deposits in Yili Basin, Xinjiang, and their implications for provenance environmental*. [dissertation/master's thesis]. Fuzhou: Fujian Normal University (in Chinese).
- Jiang, Z., Sun, Z., Liu, Z., Cao, H., Geng, W., Xu, H., et al. (2019). Rare-Earth element geochemistry reveals the provenance of sediments on the southwestern margin of the Challenger Deep. *J. Ocean. Limnol.* 37, 998–1009. doi:10.1007/s00343-019-8046-8
- Kang, S., Wang, X., Wang, N., Song, Y., Liu, W., Wang, D., et al. (2022). Siberian high modulated suborbital-scale dust accumulation changes over the past 30 ka in the eastern yili basin, central asia. *Paleoceanog Paleoclimatol* 37. doi:10.1029/2021PA004360
- Laveuf, C., and Cornu, S. (2009). A review on the potentiality of Rare Earth Elements to trace pedogenetic processes. *Geoderma* 154, 1–12. doi:10.1016/j.geoderma.2009.10.002
- Lehmkuhl, F., and Haselein, F. (2000). Quaternary paleoenvironmental change on the Tibetan Plateau and adjacent areas (Western China and Western Mongolia). *Quat. Int.* 65 (66), 121–145. doi:10.1016/S1040-6182(99)00040-3
- Lehmkuhl, F., Schulte, P., Zhao, H., Hülle, D., Protze, J., and Stauch, G. (2014). Timing and spatial distribution of loess and loess-like sediments in the mountain areas of the northeastern Tibetan Plateau. *CATENA* 117, 23–33. doi:10.1016/j.catena.2013.06.008
- Li, Y., and Song, Y. (2021). Discussion of the paper “Loess gGenesis and worldwide distribution” by Yanrong Li, Wenhui Shi, Adnan Aydin, et al. *Earth-Science Rev.* 221, 103151. doi:10.1016/j.earscirev.2020.103151
- Li, Z., Wang, N., Cheng, H., and Li, Y. (2016). Early-middle Holocene hydroclimate changes in the Asian monsoon margin of northwest China inferred from Huahai terminal lake records. *J. Paleolimnol.* 55, 289–302. doi:10.1007/s10933-016-9880-8
- Li, Y. H. M., Zhao, W. W., and Zhou, M.-F. (2017). Nature of parent rocks, mineralization styles and ore Genesis of regolith-hosted REE deposits in South China: An integrated genetic model. *J. Asian Earth Sci.* 148, 65–95. doi:10.1016/j.jseaes.2017.08.004
- Li, G., Chen, F., Xia, D., Yang, H., Zhang, X., Madsen, D., et al. (2018). A Tianshan Mountains loess-paleosol sequence indicates anti-phase climatic variations in arid central Asia and in East Asia. *Earth Planet. Sci. Lett.* 494, 153–163. doi:10.1016/j.epsl.2018.04.052
- Li, Y., Shi, W., Aydin, A., Beroya-Eitner, M. A., and Gao, G. (2020a). Loess Genesis and worldwide distribution. *Earth-Science Rev.* 201, 102947. doi:10.1016/j.earscirev.2019.102947
- Li, Y., Song, Y., Fitzsimmons, K. E., Chen, X., Prud'homme, C., and Zong, X. (2020b). Origin of loess deposits in the North tian Shan piedmont, central asia. *Palaeogeogr. Palaeoclimatol. Palaeoecol.* 559, 109972. doi:10.1016/j.palaeo.2020.109972
- Li, Z., Chen, Q., Dong, S., Zhang, D., Yu, X., and Zhang, C. (2021). Applicability of rare earth elements in eolian sands from desert as proxies for provenance: A case study in the Badain Jaran Desert, northwestern China. *CATENA* 207, 105647. doi:10.1016/j.catena.2021.105647
- Li, G., Zhang, H., Liu, X., Yang, H., Wang, X., Zhang, X., et al. (2020). Paleoclimatic changes and modulation of East Asian summer monsoon by high-latitude forcing over the last 130,000 years as revealed by independently dated loess-paleosol sequences on the NE Tibetan Plateau. *Quat. Sci. Rev.* 237, 106283. doi:10.1016/j.quascirev.2020.106283
- Li, P., Zhang, C., Wu, H., and Gao, Z. (2022). Geochemical characteristics of Holocene loess-paleosol sequences in central Chinese Loess Plateau and their implications for East Asian monsoon evolution. *Quat. Int.* 616, 99–108. doi:10.1016/j.quaint.2021.10.017
- Li, Y., Song, Y., Kaskaoutis, D. G., Zhang, X., Chen, X., Shukurov, N., et al. (2022). Atmospheric dust dynamics over central asia: A perspective view from loess deposits. *Gondwana Res.* 109, 150–165. doi:10.1016/j.gr.2022.04.019
- Liang, P., Chen, B., Yang, X., Liu, Q., Li, A., Mackenzie, L., et al. (2022). Revealing the dust transport processes of the 2021 mega dust storm event in northern China. *Sci. Bull.* 67, 21–24. doi:10.1016/j.scib.2021.08.014
- Ling, Z., Wang, J., Cheng, L., and Lu, B. (2018). Rare earth elements' geochemical characteristics of nebkhas in the Qaidam Basin and the provenance. *J. Desert Res.* 38, 963–971. (in Chinese).
- Liu, J., Yao, Y., Elsworth, D., Pan, Z., Sun, X., and Ao, W. (2016). Sedimentary characteristics of the lower cambrian niutitang shale in the southeast margin of sichuan basin, China. *J. Nat. Gas Sci. Eng.* 36, 1140–1150. doi:10.1016/j.jngse.2016.03.085
- Lu, H., Wang, X., Wang, Y., Zhang, X., Yi, S., Wang, X., et al. (2022). Chinese loess and the Asian monsoon: What we know and what remains unknown. *Quat. Int.* 620, 85–97. doi:10.1016/j.quaint.2021.04.027
- Ma, B., and Li, D. (2008). Stages of the neotectonic movement of the menyuan basin in the middle segment of the qilian mountains. *J. Geomechanics* 14, 201–211. (in Chinese)
- Ma, J., Wei, G., Xu, Y., Long, W., and Sun, W. (2007). Mobilization and re-distribution of major and trace elements during extreme weathering of basalt in Hainan Island, South China. *Geochimica Cosmochimica Acta* 71, 3223–3237. doi:10.1016/j.gca.2007.03.035
- McLennan, S. M. (2018). “Geochemistry and mineralogy of rare earth elements,” eds. B. R. Lipin and G. A. McKay (Berlin: De Gruyter), 169–200. doi:10.1515/9781501509032-010
- Miao, X., Chongyi, E., Xu, S., Wang, Q., Hanson, P. R., Chen, H., et al. (2022). Age and source of coastal loess in Shandong Peninsula, Bohai Sea, China: Implications for dust aggradation in respond to sea-level change. *Aeolian Res.* 54, 100767. doi:10.1016/j.aeolia.2021.100767
- Mongelli, G. (1995). Trace elements distribution and mineralogical composition in the < 2- μ m size fraction of shales from the Southern Apennines, Italy. *Mineralogy Petrology* 53, 103–114. doi:10.1007/BF01171949
- Moreno Chamarro, E., Marshall, J., and Delworth, T. L. (2020). Linking ITCZ migrations to the AMOC and North Atlantic/pacific SST decadal variability. *J. Clim.* 33, 893–905. doi:10.1175/JCLI-D-19-0258.1
- Muhs, D. R. (2013). “11.9 loess and its geomorphic, stratigraphic, and paleoclimatic significance in the quaternary,” in *Treatise on geomorphology*. Editor J. F. Shroder (San Diego: Academic Press), 149–183. doi:10.1016/B978-0-12-374739-6.00302-X

- Nesbitt, H. W., and Young, G. M. (1982). Early Proterozoic climates and plate motions inferred from major element chemistry of lutites. *Nature* 299, 715–717. doi:10.1038/299715a0
- Nesbitt, H. W. (1979). Mobility and fractionation of rare earth elements during weathering of a granodiorite. *Nature* 279, 206–210. doi:10.1038/279206a0
- Obrecht, I., Zeeden, C., Schulte, P., Hambach, U., Eckmeier, E., Timar-Gabor, A., et al. (2015). Aeolian dynamics at the Orlovat loess–paleosol sequence, northern Serbia, based on detailed textural and geochemical evidence. *Aeolian Res.* 18, 69–81. doi:10.1016/j.aeolia.2015.06.004
- Pye, K. (1995). The nature, origin and accumulation of loess. *Quat. Sci. Rev.* 14, 653–667. doi:10.1016/0277-3791(95)00047-X
- Ramos, S. J., Dinali, G. S., Oliveira, C., Martins, G. C., Moreira, C. G., Siqueira, J. O., et al. (2016). Rare earth elements in the soil environment. *Curr. Pollut. Rep.* 2, 28–50. doi:10.1007/s40726-016-0026-4
- Reichow, M. K., Saunders, A. D., White, R. V., Al'Mukhamedov, A. I., and Medvedev, A. Y. (2005). Geochemistry and petrogenesis of basalts from the west siberian basin: An extension of the permo–triassic siberian traps, Russia. *Lithos* 79, 425–452. doi:10.1016/j.lithos.2004.09.011
- Ren, H., and Pan, X. (2019). *Integration dataset of tibet plateau boundary*. China: National Tibetan Plateau Data Center. doi:10.11888/Geogra.tpcd.270099
- Romero, M., Torre, G., and Gaiero, D. M. (2021). Palaeoenvironmental changes in southern South American dust sources during the last glacial/interglacial transition: Evidence from clay mineral assemblages of the pampean loess. *Quat. Int.* 580, 11–21. doi:10.1016/j.quaint.2020.12.044
- Rudnick, R. L., and Gao, S. (2003). “Composition of the continental crust,” in *Treatise on geochemistry* (Netherlands: Elsevier), 1–64. doi:10.1016/B0-08-043751-6/03016-4
- Shi, Y., E, C., Zhang, J., Sun, M., Li, P., Peng, Q., et al. (2021). Environmental implications of magnetic susceptibility of the loess at different altitudes in Qinghai Lake area. *J. Earth Environ.* 12, 256–268. (in Chinese). doi:10.7515/JEE212006
- Skurzynski, J., Jary, Z., Kenis, P., Kubik, R., Moska, P., Raczky, J., et al. (2020). Geochemistry and mineralogy of the Late Pleistocene loess-paleosol sequence in Złota (near Sandomierz, Poland): Implications for weathering, sedimentary recycling and provenance. *Geoderma* 375, 114459. doi:10.1016/j.geoderma.2020.114459
- Song, Y., Chen, X., Qian, L., Li, C., Li, Y., Li, X., et al. (2014). Distribution and composition of loess sediments in the ili basin, central asia. *Quat. Int.* 334 (335), 61–73. doi:10.1016/j.quaint.2013.12.053
- Song, Y., Li, Y., Cheng, L., Zong, X., Kang, S., Ghafarpour, A., et al. (2021). Spatiotemporal distribution of quaternary loess across central asia. *Palaeogeogr. Palaeoclimatol. Palaeoecol.* 567, 110279. doi:10.1016/j.palaeo.2021.110279
- Stauch, G., Jmker, J., Pötsch, S., Zhao, H., Hilgers, A., Diekmann, B., et al. (2012). Aeolian sediments on the north-eastern Tibetan Plateau. *Quat. Sci. Rev.* 57, 71–84. doi:10.1016/j.quascirev.2012.10.001
- Sun, S. S., and McDonough, W. F. (1989). Chemical and isotopic systematics of oceanic basalts: Implications for mantle composition and processes. *SP 42*, 313–345. doi:10.1144/GSL.SP.1989.042.01.19
- Sun, Y., Clemens, S. C., An, Z., and Yu, Z. (2006). Astronomical timescale and palaeoclimatic implication of stacked 3.6-Myr monsoon records from the Chinese Loess Plateau. *Quat. Sci. Rev.* 25, 33–48. doi:10.1016/j.quascirev.2005.07.005
- Sun, Y., Yin, Q., Crucifix, M., Clemens, S. C., Araya-Melo, P., Liu, W., et al. (2019). Diverse manifestations of the mid-Pleistocene climate transition. *Nat. Commun.* 10, 352. doi:10.1038/s41467-018-08257-9
- Sun, Y., Yan, Y., Nie, J., Li, G., Shi, Z., Qiang, X., et al. (2020). Source-to-sink fluctuations of Asian aeolian deposits since the late Oligocene. *Earth-Science Rev.* 200, 102963. doi:10.1016/j.earscirev.2019.102963
- Sun, J. (2002). Provenance of loess material and formation of loess deposits on the Chinese Loess Plateau. *Earth Planet. Sci. Lett.* 203, 845–859. doi:10.1016/S0012-821X(02)00921-4
- Tan, H., Ma, H., Zhang, X., Lu, H., and Wang, J. (2006). Typical geochemical elements in loess deposit in the northeastern Tibetan Plateau and its paleoclimatic implication. *Acta Geol. Sin. - Engl. Ed.* 80, 110–116. doi:10.1111/j.1755-6724.2006.tb00800.x
- Taylor, S. R., and McLennan, S. M. (1985). *The continental crust: Its composition and evolution*. United States: Blackwell Scientific Pub.
- Thorpe, M. T., Hurowitz, J. A., and Dehouck, E. (2019). Sediment geochemistry and mineralogy from a glacial terrain river system in southwest Iceland. *Geochimica Cosmochimica Acta* 263, 140–166. doi:10.1016/j.gca.2019.08.003
- Wall, F. (2014). Rare Earth elements. *Crit. Met. Handb.*, 312–339. doi:10.1002/9781118755341.ch13
- Wang, Y., and Zhang, Z. (1980). *Loess in China*. China: Xi'an: Shaanxi People's Art Publishing House. (in Chinese).
- Wang, X., Vandenberghe, D., Yi, S., Vandenberghe, J., Lu, H., Van Balen, R., et al. (2013). Late Quaternary paleoclimatic and geomorphological evolution at the interface between the Menyuan basin and the Qilian Mountains, northeastern Tibetan Plateau. *Quat. Res.* 80, 534–544. doi:10.1016/j.yqres.2013.08.004
- Wang, G., Wang, Y., Wei, Z., He, W., Zhang, T., and Ma, X. (2020). Geochemical records of Qinghai Lake sediments in southwestern China linked to late Quaternary climate changes. *Palaeogeogr. Palaeoclimatol. Palaeoecol.* 560, 109902. doi:10.1016/j.palaeo.2020.109902
- Wang, Y., Guo, F., Ma, L., Yan, Y., Liu, X., and Sun, Y. (2020). Millennial-scale summer monsoon oscillations over the last 260 ka revealed by high-resolution elemental results of the Mangshan loess-paleosol sequence from the southeastern Chinese Loess Plateau. *Quat. Int.* 552, 164–174. doi:10.1016/j.quaint.2020.05.039
- Wang, J. (2013). *The map of desert distribution in 1:2,000,000 in China*. China: National Tibetan Plateau Data Center. doi:10.3972/westdc.009.2013.db
- Wei, T., Dong, Z., Kang, S., and Ulbrich, S. (2018). Tracing the provenance of long-range transported dust deposition in cryospheric basins of the northeast Tibetan plateau: REEs and trace element evidences. *Atmosphere* 9, 461. doi:10.3390/atmos9120461
- Wei, H., E, C., Zhang, J., Sun, Y., Li, Q., Hou, G., et al. (2020). Climate change and anthropogenic activities in Qinghai Lake basin over the last 8500 years derived from pollen and charcoal records in an aeolian section. *CATENA* 193, 104616. doi:10.1016/j.catena.2020.104616
- Xie, X., Liu, X., Chen, G., and Korty, R. L. (2019). A transient modeling study of the latitude dependence of east Asian winter monsoon variations on orbital timescales. *Geophys. Res. Lett.* 46, 7565–7573. doi:10.1029/2019GL083060
- Xu, C., E, C., Shi, Y., Zhang, J., Sun, M., Zhang, Z., et al. (2022). Holocene aeolian activity recorded by mountain paleosols, gonghe basin, northeast qinghai-tibet plateau. *Front. Earth Sci.* 10. doi:10.3389/feart.2022.832993
- Yang, M., Liang, X., Ma, L., Huang, J., He, H., and Zhu, J. (2019). Adsorption of REEs on kaolinite and halloysite: A link to the REE distribution on clays in the weathering crust of granite. *Chem. Geol.* 525, 210–217. doi:10.1016/j.chemgeo.2019.07.024
- Yang, S., Luo, Y., Li, Q., Liu, W., Chen, Z., Liu, L., et al. (2021). Comparisons of topsoil geochemical elements from Northwest China and eastern Tibetan Plateau identify the plateau interior as Tibetan dust source. *Sci. Total Environ.* 798, 149240. doi:10.1016/j.scitotenv.2021.149240
- Yu, L., and Lai, Z. (2012). OSL chronology and palaeoclimatic implications of aeolian sediments in the eastern Qaidam Basin of the northeastern Qinghai-Tibetan Plateau. *Palaeogeogr. Palaeoclimatol. Palaeoecol.* 337–338, 120–129. doi:10.1016/j.palaeo.2012.04.004
- Zhang, X. Y., Gong, S. L., Zhao, T. L., Arimoto, R., Wang, Y. Q., and Zhou, Z. J. (2003). Sources of asian dust and role of climate change versus desertification in asian dust emission: Asian dust sources. *Geophys. Res. Lett.* 30. doi:10.1029/2003GL018206
- Zhang, H., Zhang, W., Chang, F., Yang, L., Lei, G., Yang, M., et al. (2009). Geochemical fractionation of rare earth elements in lacustrine deposits from Qaidam Basin. *Sci. China Ser. D Earth Sci.* 52, 1703–1713. doi:10.1007/s11430-009-0097-9
- Zhang, W., Zhao, J., Chen, J., Ji, J., and Liu, L. (2018). Binary sources of Chinese loess as revealed by trace and REE element ratios. *J. Asian Earth Sci.* 166, 80–88. doi:10.1016/j.jseas.2018.07.017
- Zhang, H., Lu, H., He, J., Xie, W., Wang, H., Zhang, H., et al. (2022). Large-number detrital zircon U-Pb ages reveal global cooling caused the formation of the Chinese Loess Plateau during Late Miocene. *Sci. Adv.* 8, eabq2007. doi:10.1126/sciadv.abq2007
- Zhang, H., Li, J., Ma, Y., Cao, J., and Wang, N. (1997). A study on elemental geochemical characters of the Wuwei loess section in the south vicinity of Tengger Desert. *Acta Sedimentol. Sin.* 15, 152–158. (in Chinese).
- Zhang, W., Wu, J., Zhan, S., Pan, B., and Cai, Y. (2021). Environmental geochemical characteristics and the provenance of sediments in the catchment of lower reach of Yarlung Tsangpo River, southeast Tibetan Plateau. *CATENA* 200, 105150. doi:10.1016/j.catena.2021.105150
- Zhang, X., Zhang, H., Chang, F., Xie, P., Li, H., Wu, H., et al. (2021). Long-range transport of aeolian deposits during the last 32 kyr inferred from rare earth elements and grain-size analysis of sediments from Lake Lugu, Southwestern China. *Palaeogeogr. Palaeoclimatol. Palaeoecol.* 567, 110248. doi:10.1016/j.palaeo.2021.110248
- Zhang, X. Y., Arimoto, R., and An, Z. S. (1997). Dust emission from Chinese desert sources linked to variations in atmospheric circulation. *J. Geophys. Res.* 102, 28041–28047. doi:10.1029/97JD02300